Optimal LES and a New Near-Wall Model for Application to High-Reynolds-Number Air Foils

Final Report for Contract F9550-07-1-0411

R. D. Moser
Institute for Computational Engineering and Sciences and
Department of Mechanical Engineering
University of Texas at Austin
Austin, TX 78712

1 Motivation and Objectives

One of the most promising techniques for the prediction of turbulent flows is Large Eddy Simulation (LES), in which the largest scales of turbulent fluid motion are simulated while the effect of the smaller unresolved scales are modeled. However, one of the major obstacles to the use of LES in technologically important turbulent flows, such as the flow over an airfoil, is the modeling of the near-wall turbulence. Current LES modeling approaches require that either the near-wall turbulence be adequately resolved (at unacceptable expense for large Reynolds numbers), or that an LES wall-model be used, which to date has not provided accurate results in relatively complex flows (e.g. an airfoil near stall).

A new modeling approach for wall-bounded turbulence has been developed, which promises to address the wall-modeling problem described above. It is based on a formal filtering of the turbulence *and* the boundary, a determination of the wall stress to minimize the "leakage" of kinetic energy and momentum from the flow domain, and the use of the optimal LES formulation. These three ingredients have been shown to produce accurate LES results in a turbulent channel. Further, each of these modeling formulations is generally applicable, so they can be expected to provide a basis for successful wall modeling in more complex flow situations, such as the flow over an airfoil.

The objective of this research was thus to further refine and validate this wall-modeling approach, and ultimately apply it to the flow over an airfoil. To accomplish this, we pursued a number of intermediate objectives:

- Completion and testing of the optimal LES (OLES))finite volume formulation using only theoretical inputs. Such theory-based OLES is necessary so that the models will be predictive (i.e. will not need empirical inputs).
- Refinement and generalization of an approximation of the multi-point correlations in wall-bounded turbulence. A formulation for the anisotropy and inhomogeneity of the correlations

REPORT DOCUMENTATION PAGE

Form Approved
OMB No. 0704-0188

PLEASE DO NOT RETURN YOUR FORM TO THE ABOVE ORGANIZATION.

1. REPORT DATE *(DD-MM-YYYY)*	2. REPORT TYPE	3. DATES COVERED *(From - To)*
07/04/2010	Final	12/1/2006 - 11/30/2009

4. TITLE AND SUBTITLE
Optimal LES and a New Near-Wall Model for Application to High-Reynolds-Number Air Foils

5a. CONTRACT NUMBER
F9550-07-1-0411

5b. GRANT NUMBER

5c. PROGRAM ELEMENT NUMBER

6. AUTHOR(S)
Robert D. Moser

5d. PROJECT NUMBER

5e. TASK NUMBER

5f. WORK UNIT NUMBER

7. PERFORMING ORGANIZATION NAME(S) AND ADDRESS(ES)
University of Texas at Austin
1 University Station,
Austin TX, 78712

8. PERFORMING ORGANIZATION REPORT NUMBER

9. SPONSORING/MONITORING AGENCY NAME(S) AND ADDRESS(ES)
Air Force Office of Scientific Research
875 North Randolph Street Suite 325, Room 3112
Arlington, Virginia 22203

10. SPONSOR/MONITOR'S ACRONYM(S)
AFOSR

11. SPONSOR/MONITOR'S REPORT NUMBER(S)

12. DISTRIBUTION/AVAILABILITY STATEMENT
Approved for Public Release

13. SUPPLEMENTARY NOTES

14. ABSTRACT

Three primary results of research to extend applicability of optimal large eddy simulation (OLES) to general wall-bounded flows are reported. These are: 1) the formulation and testing of theoretically-based OLES, in which theory for multi-point velocity correlations replaces emperical data as input to the model; 2) development of anisotropic models of the two-point correlation for use in wall-bounded OLES; and, 3) generalization and testing of finite-volume OLES formulations to wall-bounded turbulence. It was found that theoretically-based OLES performs very well. The anisotropy representation was formulated in terms of structure tensors, and this also provided a very good representation of the anisotropy in wall-bounded turbulence. But the approach was judged to be too complex for use with the correlations needed in OLES, and a simpler approach is proposed. Finally, the finite-volume OLES for wall-bounded turbulence resulted in a problem that arises from the treatement of the pressure and incompressibility. A new OLES formulation designed to address this has been developed and is being tested.

15. SUBJECT TERMS
Turbulence, Large Eddy Simulation, Turbulence Modeling

16. SECURITY CLASSIFICATION OF:			17. LIMITATION OF ABSTRACT	18. NUMBER OF PAGES	19a. NAME OF RESPONSIBLE PERSON
a. REPORT	b. ABSTRACT	c. THIS PAGE			Robert D. Moser
U	U	U	UU	37	19b. TELEPHONE NUMBER *(Include area code)* 512-471-3168

Reset

Standard Form 298 (Rev. 8/98)
Prescribed by ANSI Std. Z39.18
Adobe Professional 7.0

is needed to apply the theoretical formulation described above for strongly inhomogeneous turbulence as occurs nears walls.

- Generalization of the wall-bounded formulation used in [6] to the finite volume OLES formulation, which is appropriate for use in general geometries.
- Application of the above OLES generalizations to general wall-bounded flows.

2 Background and Approach

It is well known that our ability to predict complex fluid flows is limited by the need to model the effects of turbulence. For example, Reynolds averaged (RANS) turbulence models have difficulties in flows exhibiting large separation and vortex shedding. Thus, in the technologically critical problem of flow over an airfoil, there remains a great need to improve turbulence predictive techniques, especially at large angle of attack. Large eddy simulation (LES) is increasingly being employed to avoid the weaknesses of RANS models, and to provide more information than RANS computations are able to provide (e.g. for aeroacoustic phenomena or unsteady forces). However, LES remains prohibitively expensive for high Reynolds number applications, including airfoils, largely due to the treatment of walls [31, 23].

Recently, a European consortium undertook to evaluate current capabilities of LES for application to airfoils [23]. A high lift airfoil at angle of attack sufficient to produce a mild separation on the suction side toward the trailing edge was simulated by a variety of groups, using an array of different LES modeling techniques. In this study, it was found that with current LES techniques, it was necessary to resolve the near-wall turbulence to obtain accurate results. LES performed with wall function representations of the near-wall region were not satisfactory.

The cost implications of resolving the near wall layer are severe, with classical estimates for simulating the boundary layer (as on an airfoil) in LES yielding costs that scale with $Re_c^{0.5}$ if the near-wall layer is not resolved, versus $Re_c^{2.4}$ if the near-wall layer must be resolved, as suggested above [34, 10]. The reason for the difference is that resolution of the near-wall layer requires grid sizes that scale with the viscous wall unit (ν/u_τ, where u_τ is the friction velocity, defined in terms of the mean wall shear stress $u_\tau^2 = \tau_w/\rho$), which get small relative to the boundary layer thickness approximately like Re^{-1}. As a result, such wall-resolving LES have only been performed for airfoils at moderate Reynolds numbers, with very narrow spanwise domains. For example, [22] used a spanwise domain size of just 1.2% of chord to simulate the A-Airfoil from Aérospatiale at a chord Reynolds number of 2.1×10^6. Wall-resolved LES of an actual three dimensional wing is currently out of the question.

It is clear that an LES wall modeling approach is needed that does not require the resolution of the near-wall layer, and a number of research efforts have been directed at this problem, with only limited success. For an account of these efforts, see the recent review by [31], as well as several more recent papers [41, 37] The approaches generally pose stress boundary conditions for the LES equations, and a number of modeling approaches to determine the required boundary stresses have been developed. These include the correlation of the wall stresses with large-scale velocities in the interior [32], a boundary layer representation of the wall layer [41] and the use of optimal control

to ensure that known statistical properties of the turbulence are reproduced [37, 27].

Under a previous AFOSR/NSF jointly funded project, a new approach to the wall-modeling problem was shown to yield remarkably good results in turbulent channel flow [11, 25]. This approach is based on the observation that in an LES, it is not consistent to identify the location of anything, including a no-slip boundary, to more accuracy than the filter width, suggesting that the wall should be filtered as well as the turbulence in the interior. This approach provides a formal basis for the introduction of the wall stress in the LES equations, and by including the region exterior to the flow domain in the computation, it allows the wall stresses to be determined by ensuring that momentum and energy do not "leak" from the flow domain. This simple and very general modeling ansatz appears to be sufficient to provide LES boundary conditions.

However, even with an accurate representation of wall stresses, a model is needed for the subgrid effects in the flow domain interior that is valid near the wall (in the log layer), where the assumptions of small scale isotropy and scale similarity, on which most subgrid models are based, are not valid. Fortunately, the optimal LES approach pursued over the years in our group is valid even in the absence of small-scale isotropy and scale similarity. Optimal LES models were used in conjunction with the filtered boundary/no leakage boundary model, to produce the encouraging results described above.

Application of optimal LES to wall bounded turbulence in conjunction with the flitered wall/no-leakage wall stress model will be enabling for LES of complex wall-bounded flows. The effectiveness of the OLES formalism in this application was demonstrated previously by appealing to DNS statistical data for required modeling inputs, but to use it in applications requires that the need for empirical data be eliminated. This can be done using theory for the multi-point correlations of turbulence [26]. When small-scale isotropy is valid, Kolmogorov inertial range scaling and mild modeling assumptions allow the required correlations to be determined, and the resulting models need to be evaluated and tested. For anisotropic inhomogeneous turbulence, a generalization of these correlation models is needed. An approach based on the structure tensor representation of anisotropy was proposed earlier. Here, we generalize and evaluate that approach for use in wall-bounded turbulence. Finally, previous applications of OLES to wall bounded flows were based on a spectral representation of the LES velocity fields [39, 5]. To support complex flow domains, the finite-volume formulation of OLES needs to be applied to wall-bounded turbulence. These developments have been pursued in preparation for application of OLES in complex wall-bounded turbulent flows.

3 Supported Research

To pursue the objectives defined above, a number of research activities were pursued under the current grant. These are described briefly below and in more detail in the following subsections, and the referenced publications.

1. **Theoretical OLES Refinement & Testing**: The most difficult statistical input to determine theoretically for the OLES formulation is the three-point third-order velocity correlation tensor. A recent development by Chang & Moser [9], provides such a model, and so here,

OLES based on this theoretical model has been formulated and tested. Further, an asymptotic analysis for small LES filter width compared to the large scales of turbulence, produces a particularly simple Finite-Volume OLES model, which can be expressed as a finite-volume scheme representing unresolved turbulence.

2. **Refinement and Generalization of Anisotropy Models**: An important feature of near-wall turbulence, is that it is highly anisotropic, and inhomogeneous. The resulting anisotropy in the sub-filter scale turbulence needs to be represented, and in the OLES framework, this is done by representing anisotropy in the multi-point correlations. We use an approach for this based on the RANS structure tensors developed by Kassinos & Reynolds [14]. The resulting anisotropy represented was tested for its ability to reproduce the two-point correlation in channel flow, and it is quite good. It is also very complicated, and a potential alternative, more *ad hoc*, approach is also discussed.

3. **Generalization and Testing of Finite-Volume Wall-Bounded OLES**: Finite-volume formulations of OLES are much to be preferred over spectral formulations, that have until now been used in wall-bounded flows. Wall-bounded finite-volume OLES thus needs to be formulated and tested. Here that is done using statistical data from DNS.

3.1 Theoretical OLES Refinement & Testing

3.1.1 Finite-Volume Optimal LES

In finite-volume OLES, the LES state variables are the velocities averaged over discrete volumes. The mapping (filter) is equivalent to the application of a top-hat filter followed by sampling on a grid. The LES evolution equations are then determined from the volume averaged Navier-Stokes equations given by :

$$V^v \frac{d\overline{u}_i^v}{dt} = -\sum_s \mathcal{F}_i^s - \sum_s \mathcal{P}_i^s + \sum_s \mathcal{V}_i^s \tag{1}$$

where $\overline{u}_i^v$ is the velocity averaged over the volume v, V^v is the volume of v and $\mathcal{F}_i^s$, $\mathcal{P}_i^s$ and $\mathcal{V}_i^s$ are the convective flux, pressure force and viscous flux, respectively, for the surface s. The sums in (1) are over the faces of the volume v. The quantities appearing in (1) are defined as:

$$\overline{u}_i^v = \frac{1}{V^v}\int_v u_i \, \delta x \tag{2}$$

$$\mathcal{F}_i^s = \int_s u_i u_j n_j^s \, \delta x \tag{3}$$

$$\mathcal{P}_i^s = \int_s p n_i^s \, \delta x \tag{4}$$

$$\mathcal{V}_i^s = \int_s \nu \frac{\partial u_i}{\partial x_j} n_j^s \, \delta x \tag{5}$$

where u_i is the turbulent velocity and n_j^s is the outward-pointing unit normal to the surface s. As indicated, the integrals are over a volume v or one of the faces s bounding a volume. To distinguish the simulation quantities in an LES from the filtered real turbulence, the symbol w_i^v will be used

to represent the LES variables. The goal, of course, is for the dynamics and statistics of w_i^v to approximate those of $\overline{u}_i^v$ as closely as possible.

The evolution equation for w_i^v will be the same as that for $\overline{u}_i^v$ (1), with the fluxes replaced by models. In the context of OLES, the fluxes $\mathcal{F}_i^s$, $\mathcal{P}_i^s$ and $\mathcal{V}_i^s$ are to be modeled using stochastic estimation. For the current development, we will consider the limit of infinite Reynolds number in which the viscous flux $\mathcal{V}_i^s$ is negligible. Further, the pressure force will be treated as in Langford & Moser [20] (see section 3.1.3), so the development in this section will focus on the convective fluxes $\mathcal{F}_i^s$. These fluxes are to be modeled in terms of linear and quadratic functions of the LES state variables w_i^v. At least quadratic dependence is required here because the convective fluxes are themselves quadratic in the velocity. The estimate for the convective flux is thus of the form:

$$\mathcal{F}_i^s \approx \mathcal{A}_i(s) + \sum_{v_1} \mathcal{L}_{ij}(s, v_1) w_j^{v_1} + \sum_{v_1, v_2} \mathcal{Q}_{ijk}(s, v_1, v_2) w_j^{v_1} w_k^{v_2} \tag{6}$$

where $\mathcal{A}_i(s)$ is a constant term, $\mathcal{L}_{ij}(s, v)$ is the linear estimation kernel, and $\mathcal{Q}_{ijk}(s, v_1, v_2)$ is the quadratic estimation kernel. The range of the sums in (6) can be selected to be as large or small as desired, with the expectation that a larger range (a larger stencil) will produce more accurate results, though, as the stencil grows to include more distant and less well-correlated data, a diminishing return is expected [19]. It was found by ZLM [42] that a sum over 4 or 6 volumes was sufficient to get quite accurate LES results. In the LES performed here, a stencil is used that sums over 4 volumes (a $1 \times 1 \times 4$ stencil, see ZLM and section 3.1.3).

The minimum mean square error between the ideal LES and the estimate (6) is attained when [1, 19, 39]:

$$\langle \mathcal{F}_i^s \rangle = \mathcal{A}_i(s) + \sum_{v_1} \mathcal{L}_{ij}(s, v_1) \left\langle \overline{u}_j^{v_1} \right\rangle + \sum_{v_1, v_2} \mathcal{Q}_{ijk}(s, v_1, v_2) \left\langle \overline{u}_j^{v_1} \overline{u}_k^{v_2} \right\rangle \tag{7}$$

$$\langle \mathcal{F}_i^s \overline{u}_l^{v_3} \rangle = \mathcal{A}_i(s) \langle \overline{u}_l^{v_3} \rangle + \sum_{v_1} \mathcal{L}_{ij}(s, v_1) \left\langle \overline{u}_j^{v_1} \overline{u}_l^{v_3} \right\rangle + \sum_{v_1, v_2} \mathcal{Q}_{ijk}(s, v_1, v_2) \left\langle \overline{u}_j^{v_1} \overline{u}_k^{v_2} \overline{u}_l^{v_3} \right\rangle \tag{8}$$

$$\begin{aligned} \langle \mathcal{F}_i^s \overline{u}_l^{v_3} \overline{u}_m^{v_4} \rangle = {} & \mathcal{A}_i(s) \langle \overline{u}_l^{v_3} \overline{u}_m^{v_4} \rangle + \sum_{v_1} \mathcal{L}_{ij}(s, v_1) \left\langle \overline{u}_j^{v_1} \overline{u}_l^{v_3} \overline{u}_m^{v_4} \right\rangle \\ & + \sum_{v_1, v_2} \mathcal{Q}_{ijk}(s, v_1, v_2) \left\langle \overline{u}_j^{v_1} \overline{u}_k^{v_2} \overline{u}_l^{v_3} \overline{u}_m^{v_4} \right\rangle \end{aligned} \tag{9}$$

These equations can be solved for the estimation coefficients (kernels) $\mathcal{A}_i$, $\mathcal{L}_{ij}$ and $\mathcal{Q}_{ijk}$. The statistical correlations appearing in the estimation equations (7-9) are needed as input for the OLES procedure.

3.1.2 Theoretical Determination of Correlations

The correlations required for the OLES formulation are among the LES state variables (volume-averaged velocities) and the modeled quantities (convective fluxes). To determine them theoretically, they must be related to turbulence statistical quantities for which we have theories. This can easily be done, by writing the correlations appearing in (7-9) as integrals of multi-point velocity correlations. Three correlation tensors are needed to determine the estimation coefficients. Models

for these tensors must be provided as input to the OLES procedure. To develop these models, a number of assumptions will be made. First it is assumed that on length scales required for the analysis (i.e., several filter widths), the turbulence is both homogeneous and isotropic. Using homogeneity, the required correlations are written:

$$\mathbb{R}_{ij}(\mathbf{r}1) = \langle u_i'(\mathbf{x})u_j'(\mathbf{x}1)\rangle \tag{10}$$

$$\mathbb{T}_{ijk}(\mathbf{r}1,\mathbf{r}2) = \langle u_i'(\mathbf{x})u_j'(\mathbf{x}1)u_k'(\mathbf{x}2)\rangle \tag{11}$$

$$\mathbb{F}_{ijkl}(\mathbf{r}1,\mathbf{r}2,\mathbf{r}3) = \langle u_i'(\mathbf{x})u_j'(\mathbf{x}1)u_k'(\mathbf{x}2)u_l'(\mathbf{x}3)\rangle, \tag{12}$$

with the dependence expressed in terms of spatial separations, $\mathbf{r}i = \mathbf{x} - \mathbf{x}i$.

Second, it is assumed that the spatial separations are small enough to be within the Kolmogorov inertial range and that the Reynolds number based on the filter width is sufficiently large that it can be considered to be infinite. With these assumptions, the Kolmogorov [16, 15] expressions for the second and third-order longitudinal structure functions are valid:

$$S_2(r) = \langle (u_\parallel(\mathbf{x}) - u_\parallel(\mathbf{x}1))^2\rangle = C\epsilon^{2/3}r^{2/3} \tag{13}$$

$$S_3(r) = \langle (u_\parallel(\mathbf{x}) - u_\parallel(\mathbf{x}1))^3\rangle = -\frac{4}{5}\epsilon r \tag{14}$$

where $r = |\mathbf{r}|$ is the magnitude of the separation vector, $u_\parallel$ is the velocity component in the direction of the separation vector and C is the Kolmogorov constant. From these expressions and isotropy and continuity constraints, expressions for the two-point second- and third-order correlations can be derived:

$$\mathbb{R}_{ij}(\mathbf{r}) = u^2\delta_{ij} + \frac{C}{6}\epsilon^{2/3}r^{-4/3}(r_i r_j - 4(r)^2\delta_{ij}) \tag{15}$$

$$\mathbb{T}_{ijk}(0,\mathbf{r}) = \frac{\epsilon}{15}\left(\delta_{ij}r_k - \frac{3}{2}(\delta_{ik}r_j + \delta_{jk}r_i)\right) \tag{16}$$

The result for the second-order correlation is well known. The expression for the third-order correlation is less common, but it is a direct consequence of the 4/5 law (14) and the general isotropic form derived by von Kármán & Howarth [40] (see also [3, 24]). Further, the analysis leading to (16) is implicit to the derivation of the 4/5 law. The two-point third-order correlation in (16) is precisely the correlation needed to compute the correlation of fluxes with volume averaged velocities. However, the more general third-order three-point correlation is also needed for the correlation of three volume averaged velocities (see below).

Finally, to determine an expression for $\mathbb{F}_{ijkl}$, we invoke the quasi-normal approximation, which states that the fourth-order cumulants are zero. This implies that $\mathbb{F}$ can be expressed in terms of the two-point correlation $\mathbb{R}$:

$$\mathbb{F}_{ijkl}(\mathbf{r}1,\mathbf{r}2,\mathbf{r}3) \approx \mathbb{R}_{ij}(\mathbf{r}1)\mathbb{R}_{kl}(\mathbf{r}3-\mathbf{r}2) + \mathbb{R}_{ik}(\mathbf{r}2)\mathbb{R}_{jl}(\mathbf{r}3-\mathbf{r}1) + \mathbb{R}_{il}(\mathbf{r}3)\mathbb{R}_{jk}(\mathbf{r}2-\mathbf{r}1) \tag{17}$$

The quasi-normal approximation is infamous in turbulence because it is well-known to result in unrealizable spectra when used in two-point closure models [17, 29, 30, 21]. However, its application here in optimal LES modeling can result in no such catastrophe because the LES equations being solved are not for statistical quantities to which realizability constraints apply. Similarly, the modifications added to the quasi-normal approximation to assure realizability in two-point

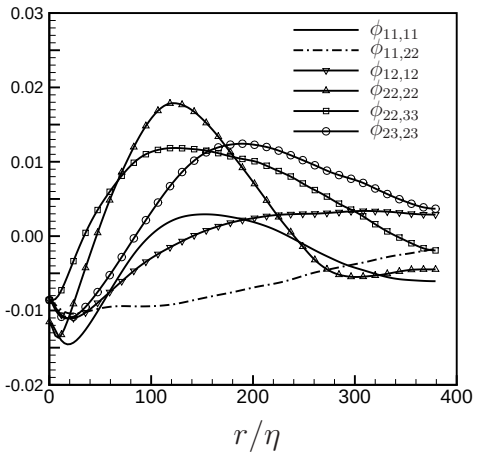

Figure 1: Relative error $\phi_{ij,kl}$ in the quasi-normal approximation to the non-zero elements of the fourth-order correlation $\mathbb{F}_{ijkl}(0, \mathbf{r}, \mathbf{r})$, with separation in the x_1 direction. To obtain ϕ, the error in $\mathbb{F}$ is normalized by $[\mathbb{F}_{ijkl}\mathbb{F}_{ijkl}(0, \mathbf{r}, \mathbf{r})]^{1/2}$. Due to isotropy the 2 and 3 indices can be swapped with identical results.

closures, such as "eddy damping" and Markovization in EDQNM [21], are applied to the evolution equation for third-order correlations. Since no such correlation evolution equations are being solved here, these refinements are not applicable. Finally, the quasi-normal approximation is generally quite accurate in isotropic turbulence [38]. For example, the error was measured in a forced isotropic turbulence DNS at $Re_\lambda = 164$ [19], and is shown in figure 1. The small magnitude of these errors does not necessarily imply that they are dynamically insignificant. Ultimately, the performance of the resulting models is the most important measure of the accuracy of these approximations (see section 3.1.3 for example LES results).

With the exception of the third-order three-point correlation, all the correlations required for the OLES model have now been defined. Unfortunately, the simple theories employed here are not sufficient to determine an expression for the three-point third-order correlation. Indeed, just writing down the most general isotropic form satisfying continuity constraints is difficult [33]. Based on this most general form, Chang & Moser [9] developed a model for $\mathbb{T}_{ijk}(\mathbf{r}^1, \mathbf{r}^2)$ for stationary, incompressible, homogeneous, isotropic turbulence for separations $\mathbf{r}^1$ and $\mathbf{r}^2$ in the inertial range, and under the assumptions of small scale isotropy and infinite Reynolds number. This model is algebraically very complex, with more than 758 terms, so it will not be written here. Computer programs to evaluate the tensor numerically are available at http://turbulence.ices.utexas.edu.

3.1.3 Testing Theoretical Optimal LES

To assess the validity of the theoretically determined correlations for use in OLES models, several of the simulations performed by ZLM [42] were repeated with the theoretically determined correlations in place of the DNS-determined correlations used by ZLM. The details of these simulations are given briefly below.

The simulations were performed for forced isotropic turbulence, using a finite-volume OLES formulation like that described here and, in more detail, in ZLM [42]. As described in section 3.1.1, three fluxes need to be estimated. The convective flux $\mathcal{F}$, the pressure force $\mathcal{P}$ and the viscous flux $\mathcal{V}$. In these simulations, the viscous fluxes are zero, consistent with the infinite-Reynolds number assumption used for the convective fluxes. As described by Langford & Moser [20] and as implemented by ZLM [42], the pressure force is determined by imposing an approximate divergence-free constraint, which is consistent with the second-order staggered grid finite-volume divergence operator. This is an optimal representation of divergence [20], which minimizes the expected error incurred by imposing an approximate divergence-free constraint.

The primary model to be considered here is that for the convective fluxes $\mathcal{F}$. The theoretical models described in section 3.1.2 for the multi-point correlations were integrated numerically to determine the correlations used in the estimation equations (7–9).

The integrals need to be performed for each combination of volumes and surface in the stencil and for each velocity component in the stencil. The stencil used here is a $1 \times 1 \times 4$ simple stencil on a staggered grid, which is stencil S4 as described by ZLM [42]. This stencil was selected because ZLM found that it is the smallest that yields good *a posteriori* results. Because the stencil is defined on a staggered grid, its definition is somewhat complicated. See Appendix B in [42] and [26] for a complete description.

Since the advent of the dynamic procedure in LES modeling [13], it has been common practice to seek ways in which LES model parameters can be determined from the LES in which they are being used. This has the advantage of eliminating adjustable model constants and allowing the model to respond to the particular details of the flow. In the OLES models developed here, only those model parameters that are clearly flow-dependent (i.e. velocity variance u^2 and dissipation rate ϵ) are treated dynamically, while the other constants that appear in the formulation, such as the Kolmogorov constant, which is given its usual value $C \approx 2$, are treated as universal constants. Setting these quantities directly reduces both the complexity of the simulations and the chance that the process of determining the constants will introduce spurious dynamics into the simulation.

Using the correlations derived from our theory, it is straightforward to dynamically determine estimates of $u^2 = 2k/3$ and ϵ in a running LES. That is what is done here, with the values being set at each time step (see [26] for details) The error in the dynamically determined value for the dissipation, ϵ_{est}, computed using filtered data from a DNS at $Re_\lambda = 164$ [19] is shown in figure 2. When the separation r is in the inertial range, $\epsilon_{\rm est}$ is within a percent of the value determined directly from the DNS ($\epsilon_{\rm DNS}$).

3.1.4 Asymptotic Optimal LES Models

The estimation equations can be solved asymptotically for small $\gamma = \Delta\epsilon/u^3$. Use of the lowest order asymptotic kernels simplifies the LES model because it removes the γ dependence of the kernels. Then, even when u^2 and ϵ are being determined dynamically, the scaled kernels do not change. Indeed, the lowest order quadratic kernel $\tilde{\mathcal{Q}}^0$ is scaled only with Δ, so, even when unscaled, the kernel only depends on the geometry of the cells being used to estimate the fluxes, and not u^2 and ϵ. In this way, the asymptotic quadratic kernel can be thought of as a finite-volume

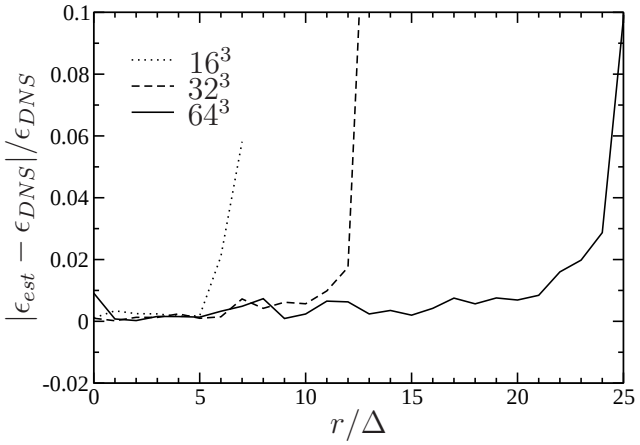

Figure 2: Relative error in estimating the dissipation from the longitudinal third-order structure function of a finite-volume filtered velocity field. Filtered structure functions were computed by filtering the DNS at $Re_\lambda = 164$ of [19]. The filter was defined on a cubical finite volume grid of the size noted, on a periodic domain of size 2π. Each finite volume is of size Δ, and r is the offset between the volumes used to compute the structure function.

v_1	$\tilde{\mathcal{L}}^0_{nn}(s, v_1)$	$\tilde{\mathcal{L}}^0_{tt}(s, v_1)$
2	0.05764	0.02623
1	-0.39059	-0.12768

Table 1: Values of the elements of $\tilde{\mathcal{L}}^0$ as determined for the $1 \times 1 \times 4$ stencil, with volume labels as defined in figure 3. The value of $\tilde{\mathcal{L}}^0$ for volumes not listed here are determined from the symmetry $\tilde{\mathcal{L}}^0_{\alpha\alpha}(s, -v_1) = -\tilde{\mathcal{L}}^0_{\alpha\alpha}(s, v_1)$.

scheme for the quadratic terms that is consistent with the statistics of turbulence. In addition to exploring the performance of theoretical OLES using the full kernels, determined without asymptotic approximation (the finite-γ kernels), the performance of the lowest order asymptotic models will be evaluated.

The asymptotic solution for the kernels is easier to understand when applied to the "simple" optimal models employed here. Because of isotropy, we need only consider the velocity component normal to the face through which the flux is being estimated and a generic velocity component tangential to the face being considered. In what follows, these components will be denoted with subscript n and t respectively (repeated n and t do not imply summation). For simple OLES models, flux of normal momentum is estimated in terms of quadratic products of the form $u_n u_n$ and linear dependence on u_n only. Tangential fluxes are estimated with quadratic and linear terms of the form $u_n u_t$ and u_t, respectively. As a consequence, the only quadratic kernel elements are $\tilde{\mathcal{Q}}_{nnn}$ and $\tilde{\mathcal{Q}}_{tnt}$, and the linear kernel elements are $\tilde{\mathcal{L}}_{\alpha\alpha}$, where the subscript α can be either n or t, and no summation is implied.

Values of the scaled asymptotic kernel elements are given in table 1 and 2 for the $1 \times 1 \times 4$ stencil. In these tables, the volume labels are as defined in figure 3, for estimates of the flux through the

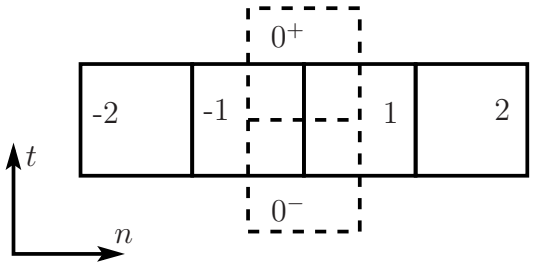

Figure 3: Volumes (and their numbering) in a $1 \times 1 \times 4$ staggered grid stencil to estimate the flux through the surface between volumes -1 and 1. For the normal-component flux (n), the volumes with solid outlines are on the n-component mesh, and the dashed-outline volumes are not used. For the tangential-component flux (t), the solid volumes are on the t-component mesh, and the dashed volumes are on the n-component mesh. In tables 1, 2, the volumes are referred to by the numbers shown here, but no distinction is made between 0^+ and 0^- because the values associated with these volumes are the same.

v_1	v_2	$\tilde{\mathcal{Q}}^0_{nnn}(s, v_1, v_2)$
2	2	0.00913
2	1	-0.11485
2	-1	-0.21432
2	-2	0.04386
1	1	0.21467
1	-1	1.16690
v_1	v_2	$\tilde{\mathcal{Q}}^0_{tnt}(s, v_1, v_2)$
0	2	-0.06617
0	1	0.31617

Table 2: Values of the elements of $\tilde{\mathcal{Q}}^0$ as determined for the $1 \times 1 \times 4$ stencil, with volume labels as defined in figure 3. The value of $\tilde{\mathcal{L}}^0$ for volumes not listed here are determined from the symmetry $\tilde{\mathcal{Q}}^0_{\alpha n \alpha}(s, -v_1, -v_2) = \tilde{\mathcal{Q}}^0_{\alpha n \alpha}(s, v_1, v_2)$.

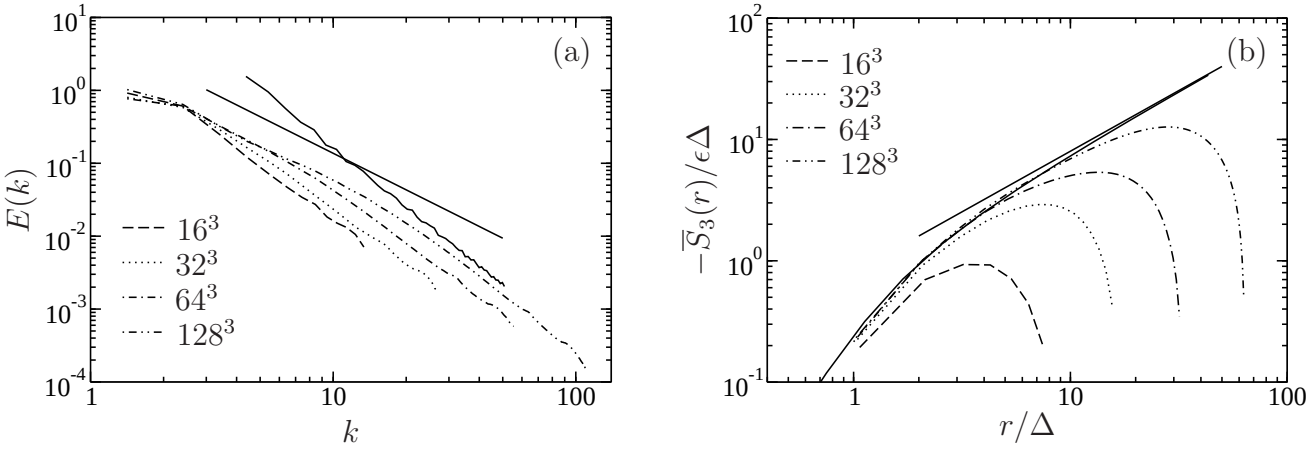

Figure 4: Three-dimensional energy spectra (a) and third-order structure functions (b) from OLES of isotropic turbulence at infinite Reynolds number using the finite-γ kernels, with resolutions ranging from 16^3 to 128^3 ($\gamma \approx 0.17$ to $\gamma \approx 0.02$, respectively). The solid lines in both plots are determined from Kolmogorov theory. In (a), the two solid lines are a $k^{-5/3}$ slope (shallow), and the result of filtering a $k^{-5/3}$ spectrum. In (b) the straight line is $S_3 = -\frac{4}{5}\epsilon r$, and the other solid line is the structure function of the filtered velocity determined from I^3.

cell face between volumes -1 and 1. The results of performing an LES with the asymptotic kernels are compared to that for the finite-γ kernels in section 3.1.5.

3.1.5 LES Results

The performance of the theory-based OLES models developed here is evaluated in isotropic turbulence at infinite Reynolds number, simulated in a periodic cube with sides of length $L = 2\pi$. The three dimensional energy spectra and third-order structure function obtained using a $1 \times 1 \times 4$ stencil [42] on a staggered grid are shown in figure 4 for different grid resolutions (16^3 to 128^3) corresponding to finite-volume filter widths varying from $\Delta \approx 0.39$ to 0.05. In these forced isotropic turbulence simulations, the energy is injected at the rate $\epsilon \approx 62.3468$, and the simulations result in a $u^2 \approx 28$, yielding $\gamma \approx 0.17$ to 0.02 for the 16^3 to 128^3 grid sizes, respectively. In all the spectra presented here, the wavenumber k is normalized by $k_{\min} = 2\pi/L$, and the three dimensional energy spectrum $E(k)$ is normalized by $\epsilon^{2/3}k_{\min}^{-5/3}$.

For all filter widths, the high wave-number portion of the LES energy spectrum exhibits a slope consistent with the filtering of a $k^{-5/3}$ inertial range. For larger grid sizes and at lower wavenumbers, the shallower $k^{-5/3}$ slope is evident, and this range becomes longer with increased resolution. This is the converged, resolution-independent part of the solution. The shifting of the filtered part of the spectrum to higher wavenumbers with increasing resolution is expected, since the filter width is being decreased. Similarly, the third-order longitudinal structure function agrees very closely with the theoretical filtered structure function obtained by integrating the third-order three-point correlation model [9] over the finite volumes. As expected, as the resolution increases, the simulation structure functions approach the $-\frac{4}{5}\epsilon r$ dependence expected in the inertial range. This

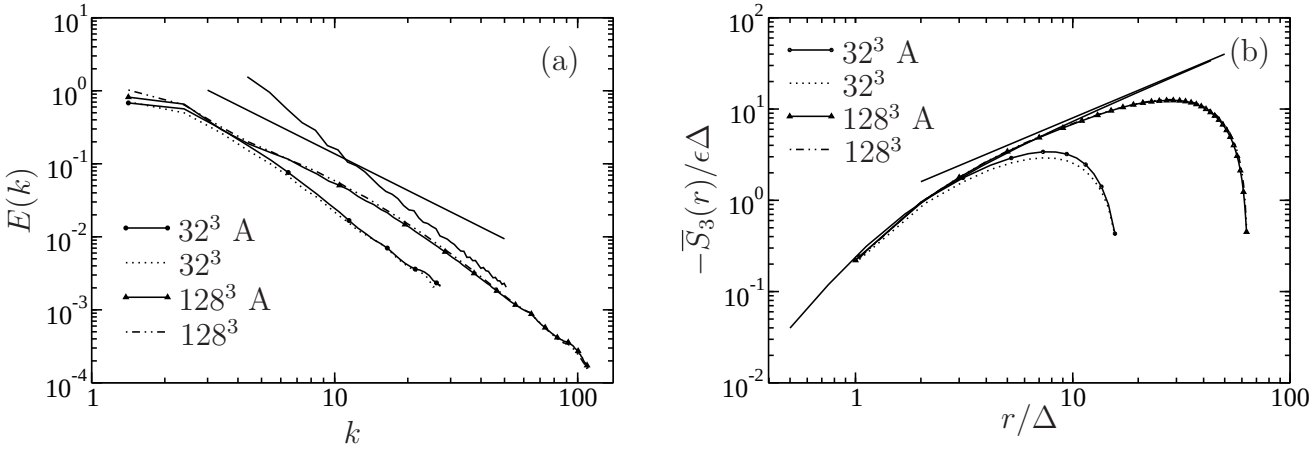

Figure 5: Three-dimensional energy spectra (a) and third-order structure functions (b) from OLES of isotropic turbulence at infinite Reynolds number using both finite γ and asymptotic kernels (signified with "A"), with resolution 32^3 and 128^3 ($\gamma = 0.08$ and $\gamma = 0.02$ respectively). Solid lines in (a) and (b) are as in figure 4.

suggests that LES is correctly representing the inertial-range energy transfer. In short, the behavior exhibited in figure 4 is precisely what is expected, indicating that the theory-based OLES model is representing the effects of the unresolved scales at infinite Reynolds number in a consistent, resolution independent way.

The LES results presented in figure 4 were obtained using the finite-γ OLES kernels, but as indicated in section 3.1.4, it will generally be more convenient to use the small-γ asymptotic kernels. A comparison of LES results from the finite-γ and asymptotic kernels is shown in figure 5. At both 128^3 and 32^3 resolutions, corresponding to $\gamma \approx 0.02$ and 0.08, respectively, the spectra and structure functions from the two cases are indistinguishable.

A finite Reynolds number case was simulated using OLES to gauge the performance of the optimal models compared to a standard model (dynamic Smagorinsky). Spectra and structure functions from these simulations are shown in figure 6 along with that from filtered DNS. Results for both $1 \times 1 \times 2$ and $1 \times 1 \times 4$ stencils on a staggered 32^3 grid are shown. With the dynamic Smagorinsky model, the two stencils correspond to second- and fourth-order schemes. Comparing the $1 \times 1 \times 4$ stencil optimal model to the corresponding dynamic model, a sharp roll-off of the spectrum at high wavenumbers is evident with the dynamic model, but not present in the optimal model. The optimal model apparently yields a better treatment of the model dissipation at high wavenumbers. However, the $1 \times 1 \times 2$ stencil optimal model does have the sharp roll-off. The optimal model spectra also have a somewhat steeper slope than either the filtered DNS or the dynamic model, but this slope is consistent with the filtered $k^{-5/3}$ spectrum. Optimal models for these stencils that are based on the DNS correlations do not exhibit this difference in slope of the spectrum between the model and filtered DNS (see ZLM [42]). It appears that the optimal model results reflect the infinite-Reynolds number theory on which the correlations are based, which is not strictly applicable to this moderate Reynolds number case. For the third-order structure function, the optimal models are somewhat more accurate in the mid-range of separations than the dynamic Smagorinsky. Otherwise, the model results are comparable.

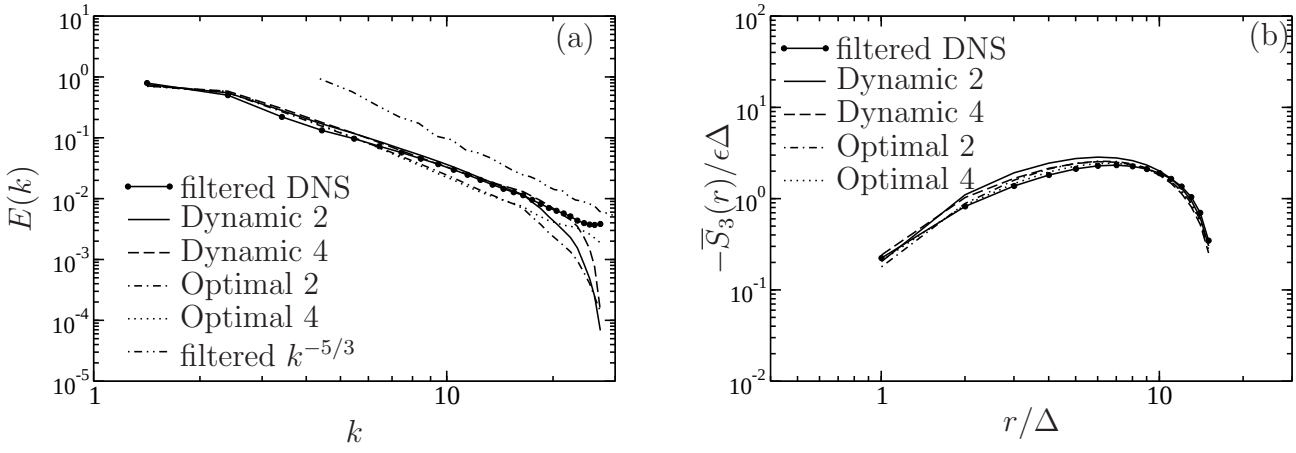

Figure 6: Three-dimensional energy spectra (a) and third-order structure function (b) from LES of isotropic turbulence on a 32^3 finite-volume grid at $Re_\lambda = 164$ using the dynamic Smagorinsky model and finite-γ optimal models, with $1 \times 1 \times 2$ and $1 \times 1 \times 4$ stencils. Also shown is a filtered DNS. Numbers on the curve labels indicate the stencil size, 2 signifies the $1 \times 1 \times 2$ stencil, 4 is the $1 \times 1 \times 4$ stencil.

At high Reynolds numbers these optimal models should yield accurate results (as seen in figure 4), and will generally be superior to the dynamic model due to the elimination of the sharp spectral roll-off near the cutoff.

3.1.6 Role of the Three-Point Third-Order Correlation

The most difficult modeling task involved in formulating the models presented here is the representation of the three-point third-order correlation. The representation for this quantity was feasible [9] only because of the assumption of small-scale isotropy. In more complex situations in which the small-scale isotropy assumption would not be valid, detailed modeling of the three-point third-order correlation will be much more difficult, if not infeasible. It is interesting, then, to consider how important this quantity is to the modeling and thus how well it needs to be known.

The primary use of the three-point correlations is in the terms that couple the equations for the quadratic and linear kernels. The coupling is most important in the equation for the linear kernels, as the coupling term in the quadratic equation is second order in $\gamma^{2/3}$. The equation for the linear kernels can be interpreted as a condition requiring that the contributions of the model to the filtered two-point correlation be the same as that for true turbulence, at least for separations included in the kernel stencil (see [19]). The critical role of I_3, the integral of the three-point correlation, then, is to measure this contribution of the quadratic part of the model. In particular, it measures the contribution of the quadratic model term to the transfer of energy to the small scales. However, the contribution to the dissipation (transfer to small scales) of the asymptotic quadratic model term is actually quite small (about 2%, see [26]). If this were generally indicative of the contribution of the I^3 terms to the estimation equations, then it would be reasonable to neglect them, greatly simplifying the modeling problem by making it largely unnecessary to develop a model for the

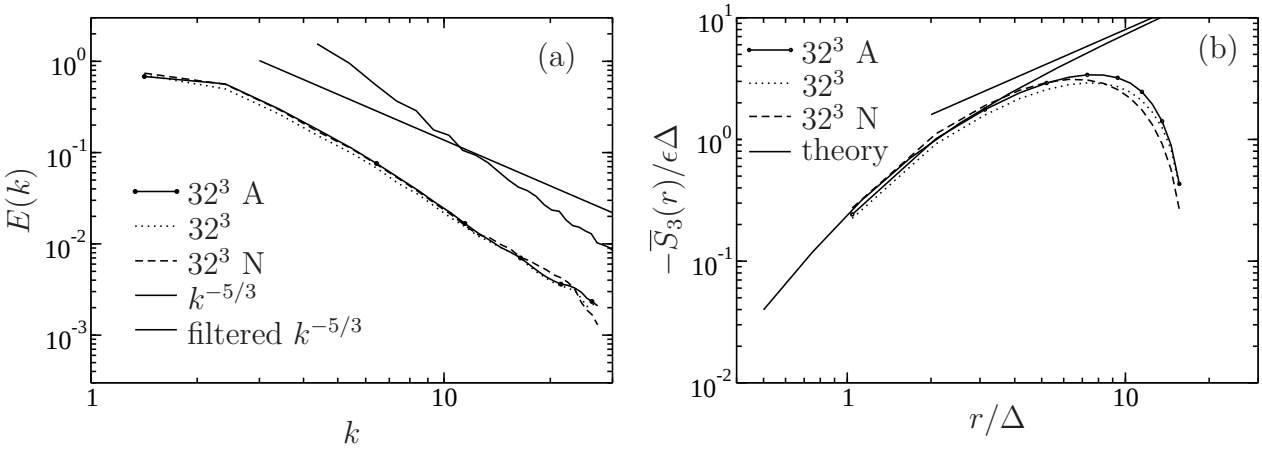

Figure 7: Three-dimensional energy spectra (a) and third-order structure functions (b) from OLES of isotropic turbulence at infinite Reynolds with resolution of 32^3 ($\gamma = 0.08$). Compared are results using the finite γ kernels, asymptotic kernels (signified with "A") and asymptotic kernels generated by neglecting the I^3 terms in the estimation equations (signified with "N"). Solid lines in (a) and (b) are as in figure 4.

three-point third-order correlation.

To explore this possibility, a set of asymptotic kernels were determined by neglecting the I^3 terms in the asymptotic estimation equations. Large eddy simulations with these modified kernels were performed, and the results for the three-dimensional spectrum and third-order structure function are shown in figure 7. The spectrum in the simulation that neglected the I^3 terms differs from that obtained with the usual asymptotic kernels in the highest octave of wavenumbers, with an up-turn followed by a sharper roll-off. This demonstrates the role of the I^3 terms in shaping the scale-distribution of the dissipation provided by the linear part of the model, in addition to the overall dissipation rate described above. The effect of neglecting the I^3 terms on the simulated third-order structure function is pronounced only at separations greater than 4Δ, for reasons that are not clear.

The importance of these differences to a practical LES can be debated. In general, whether or not the additional modeling error introduced by neglecting the I^3 terms is acceptable will depend on the goals of a particular simulation. The modest impact on the LES results in this case suggests that neglecting the I^3 terms or crudely modeling the underlying three-point third-order correlation (e.g. to account for anisotropy) may be a viable strategy in more complex flow situations. However, one must be cautious in this conclusion since in more complex situations, the quadratic operator may not behave as well, requiring a more tailored correction with the linear term, which would be determined through the I^3 terms.

3.2 Refinement and Generalization of Anisotropy Models

For a given velocity field $\mathbf{u}(\mathbf{x})$, the two-point correlation tensor R_{ij} is given by

$$R_{ij}(\mathbf{x},\mathbf{r}) = \left\langle u_i'(\mathbf{x}) u_j'(\mathbf{x}+\mathbf{r}) \right\rangle, \tag{18}$$

where $\mathbf{u}' = \mathbf{u} - \langle \mathbf{u} \rangle$ is the fluctuating velocity field. Two-point correlations of velocity fluctuations are an important ingredient of the optimal LES formulations pursued here, as discussed in the previous section. Indeed a correlation representation with a finite number of parameters can be filtered and then fit to the correlations of an LES. The resulting parameters then yield a model for the underlying unfiltered correlations. This ability to infer the correlations of $\mathbf{u}'$ from the statistics of the filtered fields is fundamental to LES, it forms the basis of subgrid modeling, and is necessary if one is to use the results of LES for analysis of turbulent flows. It is this need to represent velocity correlations in turbulent flows with complex geometries that motivates the current work.

At any given $\mathbf{x}$ location, one of the key properties of R_{ij} that needs to be represented is its anisotropy, both with regard to how different $R_{ij}(\mathbf{x},0)$ is from $R_{kk}(\mathbf{x},0)\delta_{ij}/3$, (componental anisotropy) and with regard to the elongation of the isocontours of $R_{\alpha\alpha}(\mathbf{x},\mathbf{r})$ for different directions in separation (directional anisotropy). Perhaps the most notable effort to represent this anisotropy was made in the work by Arad *et al*[2], which we will briefly describe, before discussing our motivation to pursue a different approach. In the approach taken by Arad *et al*[2], a complete basis for R_{ij} was formulated in terms of subspaces that are invariant to rigid rotation of the frame of reference, i.e. an SO(3) decomposition was proposed for $R_{ij}(\mathbf{r})$. Thus, a given second rank tensor function of $\mathbf{r}$, say $T_{ij}(\mathbf{r})$, can be expanded as $T_{ij}(\mathbf{r}) = T_{ij}(0) + \sum_{qlm} a_{qlm}(r) B_{ij}^{qlm}(\mathbf{r}/r)$ (no summation implied on repeated indices). Here, $B_{ij}^{qlm}(\mathbf{r}/r)$ are basis tensors depending only on the angular variation in $\mathbf{r}$, while $a_{qlm}(r)$ are scalar functions. For a given (l,m), the set $\{B_{ij}^{qlm}(\mathbf{r}/r); q = 1,..,N_q(l)\}$ is generated from $Y_{lm}(\mathbf{r}/r)$, the spherical harmonics, and this is a finite-dimensional subspace (i.e. $N_q(l)$ is finite for all l) that is invariant to rotational transformations. In the context of turbulent flows, for expansions of $R_{ij}(\mathbf{r})$, a power-law form was then proposed for the scalar functions, i.e. $a_{qlm}(r) = c_{qlm} r^{\xi(l)}$, and it was speculated that if $l_1 > l_2$ then $\xi(l_1) > \xi(l_2)$. The existence of a hierarchy for the power-law exponents would of course be very valuable, because at small r, the modes with lower l would dominate, and therefore $R_{ij}(\mathbf{r})$ could be well approximated with a truncated series, yielding a finite-dimensional representation.

A power law hierarchy has indeed been found in correlations constructed from DNS of homogenous turbulent flows [7]. However, DNS data of wall-bounded flows at high Reynolds number do not yield clear evidence of this hierarchy amongst the anisotropic ($l > 0$) modes[8]. A similar result was obtained when we performed SO(3) decompositions of $R_{ij}(\mathbf{r})$ computed from DNS at $\mathrm{Re}_\tau = 940$ (not shown here). Inhomogeniety in the wall-normal (y) direction is a possible reason for the lack of hierarchy of power-law exponents in wall-bounded flows. Kurien and Sreenivasan [18] accounted for the $r \sim y$ range of $R_{ij}(\mathbf{r})$ while measuring exponents in a turbulent boundary layer, and found that $\xi(2)$ was much larger than $\xi(0)$, consistent with an approach to isotropy at small scales. However, no comparison was made amongst the $l \neq 0$ exponents. Without a hierarchy in the power-law exponents, it is difficult to choose one set of SO(3) modes over others.

The abovementioned issues with the SO(3) decomposition in the context of wall-bounded flows motivated us to investigate a different approach. Here, $R_{ij}(\mathbf{r})$ is represented approximately in terms of single-point tensors, the structure tensors proposed by Kassinos *et al* [14] (referred to

below as KRR). These second-order tensors are single-point moments of derivatives of fluctuating stream functions, which can therefore be related to integrals of two-point correlations over $\mathbf{r}$. Though these tensors are single-point moments, they contain information about the "structure" of the anisotropy, e.g. the distribution of energy in different components of velocity, the dimension of turbulence, etc (discussed in [6]). Also, in the context of constructing a closure model for Reynolds stresses, it was shown by KRR that it is vital to represent the pressure-strain correlation in terms of structure tensors in order to obtain the correct evolution of the Reynolds stress components in the rapid distortion limit. The experience of KRR with the structure tensors suggests that they encode anisotropy information that is important to the evolution of the turbulence. This motivates the proposed ansatz that the anisotropy in R_{ij} be expressed in terms of structure tensors through the use of the theory of invariants [35] to construct the most general linear form.

The obvious advantage of this approach over the one by Arad *et al*[2] is that even the most general basis of tensor functions obtained here is finite-dimensional, so no power law hierarchy is needed to truncate the representation. However, unlike the SO(3) representation, the linear representaion in terms of structure tensors is not a complete basis for $R_{ij}(\mathbf{r})$. The quality of the representation depends on the validity of the modeling ansatz on which it is based. To evaluate the capabilities and shortcomings of our representation, we obtain a model for R_{ij} by fitting it to correlations obtained from DNS, and compare the two correlations (Sec. 3.2.3).

The results of this anisotropy development are described briefly below, and in more detail in [6].

3.2.1 Background

Structure tensors are single-point moments of derivatives of stream functions. The set of structure tensors that are nonzero for homogeneous turbulence are given by the Reynolds stress (or componentality) B_{ij}, dimensionality D_{ij}, circulicity F_{ij} and stropholysis $\widetilde{Q}^*_{ijk}$. In addition for inhomogeneous turbulence the inhomogeneity tensor C_{ij} is non-zero. See [14] for definitions. These tensors measure different characteristics of the anisotropy, particularly the anisotropy of the velocity components (B), the anisotropy of correlation lengths (D), the anisotropy of the vorticity components (F), the breaking of planar reflection symetries ($\widetilde{Q}$) and the anisotropy arising due to inhomogeneity (C). While these structure tensors are single-point statistical quantities, they can be expressed in terms of the two-point second-order velocity correlation, and can therefore be interpreted as measures of the anisotropy of this correlation [6].

3.2.2 A Model Form for the Homogeneous Anisotropic Two-Point Correlation

In formulating a structure-tensor based anisotropic model of the two-point correlation tensor, it will be convenient to consider an infinite Reynolds number representation for R_{ij}, with a finite Reynolds number (viscous) correction. In the limit of infinite Reynolds number, the inertial range variation of the correlations (assumed to follow a power-law) extends all the way to zero separation, where the derivatives of the correlation are then discontinuous. At finite Reynolds number, the discontinuities at $r = 0$ will be "healed" in a region of r with size of order the Kolmogorov scale η, so the finite Re correlation must diverge from the infinite Re correlation for small r (see Fig. 8).

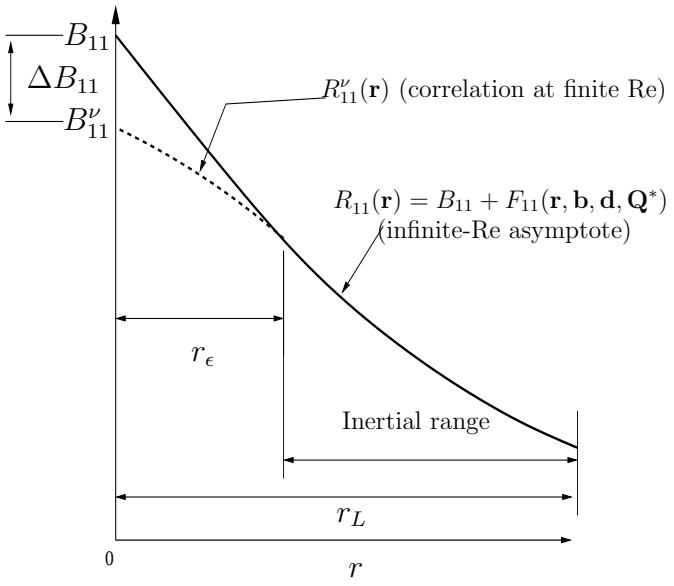

Figure 8: Schematic showing the infinite and finite-Re stream-wise correlations superimposed on each other. $R^{\nu}_{11}(\mathbf{r})$ coincides with $R_{11}(\mathbf{r})$ between $r_\epsilon < r < r_L$, but due to viscous healing peels off below $r = r_\epsilon$. The relative size of r_ϵ has been exaggerated for the sake of clarity.

To distinguish the finite and infinite Reynolds number quantities, a superscript ν will indicate the finite Reynolds version, so that:

$$R_{ij}(\mathbf{r}) = \lim_{Re\to\infty} R^{\nu}_{ij}(\mathbf{r}), \tag{19}$$

$$B_{ij} = \lim_{Re\to\infty} B^{\nu}_{ij}. \tag{20}$$

The inertial range over which the infinite Reynolds number model for $R_{ij}(\mathbf{r})$ will be valid extends over $r_\epsilon < r < r_L$, where $r_\epsilon \sim \eta \ll r_L$ and $r_L \ll \mathcal{L}$ ($\mathcal{L}$ being the length scale of the flow geometry), and the viscous healing occurs in $R^{\nu}_{ij}(\mathbf{r})$ for $r < r_\epsilon$, as shown in Fig. 8. The representation of R_{ij} in terms of structure tensors models the infinite-Re $R_{ij}(\mathbf{r})$. A weakly anisotropic finite Reynolds number correction is then introduced for $r \sim \eta$. The correction will be important when we fit our representation to finite-Reynolds number correlations computed from DNS.

In [6], it was shown that the structure tensors encode important information about the anisotropy of R_{ij}. This information is now assumed to be sufficient to reproduce the anisotropic features of the correlation in anisotropic turbulent flows. The correlation is thus assumed to depend on the structure tensors and the separation vector $\mathbf{r}$. Since we are striving to represent anisotropy, it will be convenient to re-express the dependencies in terms of the anisotropy tensors associated with $\mathbf{B}$, $\mathbf{D}$ and $\widetilde{\mathbf{Q}}^*$, which are given by

$$b_{ij} = \frac{B_{ij}}{q^2} - \frac{\delta_{ij}}{3} \tag{21}$$

$$d_{ij} = \frac{D_{ij}}{q^2} - \frac{\delta_{ij}}{3} \tag{22}$$

$$Q^*_{ijk} = \frac{\widetilde{Q}^*_{ijk}}{q^2} \tag{23}$$

where $q^2 = B_{ii}$. A model for $R_{ij}(\mathbf{r})$ of the form

$$R_{ij}(\mathbf{r}) = B_{ij} + F_{ij}(\mathbf{r}, \mathbf{b}, \mathbf{d}, \mathbf{Q}^*) \tag{24}$$

is thus sought, which is formulated so that F_{ij} goes to zero at $r = 0$. Furthermore, the function F_{ij} will be required to satisfy the following restrictions:

- The model for R_{ij} is meant for inertial range separations $r_\epsilon < r < r_L$, and our modeling assumption is that the effects of the large scale will be negligible within this range. Any fitting to DNS data will be done over only this range. Therefore, F_{ij} does not depend explicitly on r_L, and we do not explicitly model the correlation for $r > r_L$.
- The dependence on b_{ij},d_{ij} and Q^*_{ijk} is linear. This assumption is consistent with the exact linear relationship between the structure tensors and R_{ij}.
- $F_{ij}(\mathbf{r}, \mathbf{b}, \mathbf{d}, \mathbf{Q}^*)$ is invariant to proper rotation of the reference frame as well as to changes in the handedness of the axes of the reference frame.
- The symmetry $R_{ij}(\mathbf{r}) = R_{ji}(-\mathbf{r})$ is satisfied, which is exactly true for homogeneous turbulence.

The most general linear representation $F_{ij}(\mathbf{r}, \mathbf{b}, \mathbf{d}, \mathbf{Q}^*)$ is constructed using the invariant theory of tensors [35] to obtain the following form for R_{ij}:

$$R_{ij}(\mathbf{r}) = B_{ij} + R^I_{ij}(\mathbf{r}) + R^b_{ij}(\mathbf{r}, \mathbf{b}) + R^d_{ij}(\mathbf{r}, \mathbf{d}) + R^Q_{ij}(\mathbf{r}, \mathbf{Q}^*), \tag{25}$$

where,

$$\begin{aligned}
R^I_{ij}(\mathbf{r}) &= f_1(r)\delta_{ij} + f_2(r) r_i r_j, && (26)\\
R^b_{ij}(\mathbf{r}, \mathbf{b}) &= f_3(r) b_{ij} + [f_4(r)\delta_{ij} + f_5(r) r_i r_j]\mathbf{r}\cdot\mathbf{b}\cdot\mathbf{r} && (27)\\
&\quad + f_6(r)[r_i(\mathbf{r}\cdot\mathbf{b})_j + r_j(\mathbf{r}\cdot\mathbf{b})_i],\\
R^d_{ij}(\mathbf{r}, \mathbf{d}) &= f_7(r) d_{ij} + [f_8(r)\delta_{ij} + f_9(r) r_i r_j]\mathbf{r}\cdot\mathbf{d}\cdot\mathbf{r} && (28)\\
&\quad + f_{10}(r)[r_i(\mathbf{r}\cdot\mathbf{d})_j + r_j(\mathbf{r}\cdot\mathbf{d})_i],\\
R^Q_{ij}(\mathbf{r}, \mathbf{Q}^*) &= f_{11}(r)[\epsilon_{imk} Q^*_{klj} + \epsilon_{jmk} Q^*_{kli}] r_l r_m && (29)\\
&\quad + f_{12}(r)[r_j \epsilon_{ink} + r_i \epsilon_{jnk}] Q^*_{klm} r_l r_m r_n.
\end{aligned}$$

Here $f_1(r)$—$f_{12}(r)$ are scalar functions of r. The number of free scalar functions $f_i(r)$ is reduced by invoking constraints imposed by continuity and by self-consistency of the representation. In particular, a constraint is imposed that terms involving d, for example, not contribute to the componentality B or stropholysis $\widetilde{Q}$ of the model correlation, and similarly for the other terms.

The resulting constraints are:

$$\begin{aligned}
f_1' + r^2 f_2' + 4 r f_2 &= 0, && (30)\\
f_4' + 6 r f_5 + r^2 f_5' + f_6' &= 0, && (31)\\
2 r f_4 + f_3' + 5 r f_6 + r^2 f_6' &= 0, && (32)\\
f_8' + 6 r f_9 + r^2 f_9' + f_{10}' &= 0, && (33)\\
2 r f_8 + f_7' + 5 r f_{10} + r^2 f_{10}' &= 0, && (34)\\
r^2 f_{12}' + 7 r f_{12} + f_{11}' &= 0, && (35)
\end{aligned}$$

for continuity, and:

$$\frac{2b_{ij}}{15}(15g + 9rg' + r^2g'' + 35r^2f_5 + 13r^3f_5' + r^4f_5'') = 0, \quad (36)$$

$$\frac{d_{ij}}{15}(30f_7'/r + 15f_7'' + 40r^2f_9 + 20r^3f_9' + 2r^4f_9'' + 60f_{10} + 60rf_{10}' + 10r^2f_{10}'') = 0, \quad (37)$$

for self-consistency, where $g = 3f_4 + 2f_6$ (see [6] for details).

Because of the linearity of the constraints and the assumed linear dependence of R_{ij} on the structure tensors, the continuity and self-consistency constraints described above act individually on R^I, R^b, R^d and R^Q, without coupling between them. For each of these terms in the anisotropy model, the constraints leave one scalar function undetermined. We assume here that these functions are power-laws in r, consistent with the expected functional form of the correlation in the inertial range. The constraints then require that each of the four terms in the model for R_{ij} has an overall power-law dependence on the separation magnitude r, with a single exponent for each term. Call these four power-law exponents p_I, p_b, p_d and p_Q. The scalar functions $f_i(r)$ then have the form $f_i(r) = a_i r^{[p_\alpha - z_i]}$, where α is one of I, b, d, Q, depending on the term in which f_i appears and z_i is a positive integer, which is the net power of r multiplying f_i in (26)-(29). For example, $z_3 = 0$, $z_4 = 2$ and $z_5 = 4$. The coefficients a_i are also constrained, so that only four of them are independent. We choose to specify a_1, a_3, a_7 and a_{11}. Given a set of power-law exponents p_α, the ratios of the rest of the coefficients to these four coefficients are fixed by the constraints. Thus we can rewrite Eqns. (26)-(29) as:

$$R_{ij}(\mathbf{r}) = B_{ij} + \Delta R_{ij}(\mathbf{r}), \quad (38)$$

where

$$\begin{aligned}\Delta R_{ij}(\mathbf{r}) = {} & a_1 r^{p_I - 2}\left[r^2\delta_{ij} + \frac{a_2}{a_1}r_i r_j\right] \\ & + a_3 r^{p_b-4}\Big\{r^4 b_{ij} + [\frac{a_4}{a_3}\delta_{ij}r^2 + \frac{a_5}{a_3}r_i r_j]\mathbf{r}\cdot\mathbf{b}\cdot\mathbf{r} + \frac{a_6}{a_3}r^2[r_i(\mathbf{r}\cdot\mathbf{b})_j + r_j(\mathbf{r}\cdot\mathbf{b})_i]\Big\} \\ & + a_7 r^{p_d-4}\Big\{r^4 d_{ij} + [\frac{a_8}{a_7}\delta_{ij}r^2 + \frac{a_9}{a_7}r_i r_j]\mathbf{r}\cdot\mathbf{d}\cdot\mathbf{r} + \frac{a_{10}}{a_7}r^2[r_i(\mathbf{r}\cdot\mathbf{d})_j + r_j(\mathbf{r}\cdot\mathbf{d})_i]\Big\} \\ & + a_{11} r^{p_Q-4}\Big\{[\epsilon_{imk}Q^*_{klj} + \epsilon_{jmk}Q^*_{kli}]r^2 r_l r_m \\ & + \frac{a_{12}}{a_{11}}[r_j\epsilon_{ink} + r_i\epsilon_{jnk}]Q^*_{klm}r_l r_m r_n\Big\}. \end{aligned} \quad (39)$$

The above relation implies that if we fix $\{\mathbf{B}, \mathbf{b}, \mathbf{d}, \mathbf{Q}^*\}$ then there are 8 degrees of freedom (dof) in the representation, given by the four p_α and a_1, a_3, a_7, a_{11}.

At zero separation, the infinite Reynolds number inertial-range model in Eqn. (38) is equal to the infinite Reynolds number Reynolds stress B_{ij}. While the finite and infinite Reynolds number correlations will match in the inertial range, the Reynolds stress B^ν_{ij} will not, as indicated in Fig. 8. It is important to account for this difference $\Delta B_{ij} = B_{ij} - B^\nu_{ij}$ when fitting the inertial range correlation model to data from finite Reynolds number turbulence as is done in Sec. 3.2.3, or when using the model to evaluate the Reynolds stress in a turbulent flow (after fitting to an LES for

example). While $\|\Delta B_{ij}\|$ is usually small compared to B_{kk} at large Re, an incorrect estimate of B_{ij} (for instance, using $B_{ij} = B^{\nu}_{ij}$) shifts the correlation by ΔB_{ij} over all separations, including the inertial range. Thus, a good estimate of ΔB_{ij} is needed even to match the model to finite Reynolds number correlations in the inertial range.

As discussed above, $R_{ij}(\mathbf{r})$ and $R^{\nu}_{ij}(\mathbf{r})$ will correspond in the inertial range, but for sufficiently small separations ($r < r_\epsilon$), viscosity "heals" the derivative discontinuity that would be present if the inertial range behavior extended to $r = 0$. In this viscous region, the finite Re correlation can be represented as a second order Taylor series around zero, resulting in a composite representation:

$$R^{\nu}_{ij}(\mathbf{r}) = \begin{cases} B^{\nu}_{ij} + M_{ijkl} r_k r_l & \text{for } r < r_\epsilon \\ R_{ij}(\mathbf{r}) & \text{for } r > r_\epsilon \end{cases},$$

where M_{ijkl} is the tensor Taylor series coefficient. For simplicity, the matching will be done in two steps. First, r_ϵ will be determined by matching the isotropic parts of the inner and outer approximations, assuming that the isotropic parts of both approximations dominate at these small separations. For this to be a self-consistent assumption, any anisotropy in the dissipation rate tensor ϵ_{ij} must be weak, and the anisotropic power law exponents $\{p_b, p_d, p_Q\}$ must be greater than p_I. Furthermore, it is assumed that the isotropic part of the inertial range correlation satisfies Kolmogorov's 2/3 law, that is $p_I = 2/3$ and $a_1 = -2C_k\epsilon^{2/3}/3$, where $\epsilon = \epsilon_{ii}/2$ is the rate of dissipation of kinetic energy. Equating the isotropic parts of the viscous and inertial-range models at $r = r_\epsilon$, one obtains:

$$\begin{aligned} \frac{B^{\nu}_{kk}}{3}\delta_{ij} \quad - \quad & \frac{\epsilon}{15\nu} r_\epsilon^2 \left(\delta_{ij} - \frac{1}{2}\frac{r_i r_j}{r^2} \right) = \\ & \frac{B_{kk}}{3}\delta_{ij} - \frac{2C_k}{3}\epsilon^{2/3} r_\epsilon^{2/3} \left(\delta_{ij} - \frac{1}{4}\frac{r_i r_j}{r^2} \right). \end{aligned} \tag{40}$$

The value of r_ϵ is determined by matching the coefficients of $\frac{r_i r_j}{r^2}$ to obtain:

$$r_\epsilon \quad = \quad (5C_k)^{3/4}\eta. \tag{41}$$

Where $\eta = (\nu^3/\epsilon)^{1/4}$ is the Kolmogorov length scale and C_k is the Kolmogorov constant. Consistent with experimental measurements [36] a constant value of $C_k = 2$ is assumed here.

In the second step in the matching process, the correction to B_{ij} is determined by matching the inner and outer models at r_ϵ in an integral sense:

$$\int \left[B_{ij} + \Delta R_{ij}(\mathbf{r}) \right] \Big|_{r=r_\epsilon} d\angle = \int \left[B^{\nu}_{ij} + M_{ijkl} r_k r_l \right] \Big|_{r=r_\epsilon} d\angle. \tag{42}$$

Making use of the fact that

$$\lim_{r\to 0} \frac{\partial^2 R^{\nu}_{ij}(\mathbf{r})}{\partial r_k \partial r_k} = -\frac{\epsilon_{ij}}{2\nu} = 2M_{ijkk}. \tag{43}$$

and substituting Eqn. (43) and Eqn. (39) into Eqn. (42) yields:

$$B_{ij} \quad = \quad B^{\nu}_{ij} + \Delta B_{ij}, \tag{44}$$

Table 3: Specifics of the turbulent channel flow field (dimensionless)

Re_τ	940
Resolution	$3072 \times 385 \times 2304$
Box Size $(l_x/h \times l_z/h)$	$8\pi \times 3\pi$

where

$$\begin{aligned}\Delta B_{ij} &= -r_\epsilon^2 \frac{\epsilon_{ij}}{12\nu} - \frac{1}{3} r_\epsilon^{p_I} a_1 \left[3 + \frac{a_2}{a_1}\right] \delta_{ij} - \\ &\quad \frac{1}{15} r_\epsilon^{p_b} a_3 \left[15 + 2(\frac{a_5}{a_3} + 5\frac{a_6}{a_3})\right] b_{ij} - \\ &\quad \frac{1}{15} r_\epsilon^{p_d} a_7 \left[15 + 2(\frac{a_9}{a_7} + 5\frac{a_{10}}{a_7})\right] d_{ij}. \end{aligned} \quad (45)$$

Here $p_I = 2/3$ is now a fixed parameter in accordance with Kolmogorov's 2/3rd law.

3.2.3 Fitting the representation to DNS correlations

To evaluate the accuracy of the anisotropy approximation developed here, we first evaluate the free parameters in the model by fitting to correlations determined from the DNS and then compare the model to the DNS data. The fitting procedure is described in [6].

The fully developed turbulent channel flow at $Re_\tau = 940$ (Table 3) is used for the fitting and evaluation. Correlations were computed from DNS results, the details of which can be found in [12]. This is a highly inhomogeneous flow and so the extent to which the homogeneous representation is valid will also be examined.

The only direction of inhomogeneity is the one perpendicular to the channel wall. The x axis is in the stream wise direction, and the y axis is normal to the wall. The correlation can be written as $R_{ij}(y, \mathbf{r}) = \left\langle u_i'(\mathbf{x}) u_j'(\mathbf{x} + \mathbf{r}) \right\rangle |_{x_2 = y}$. The homogeneous model does not satisfy the inhomogeneous continuity equationor the symmetry of the inhomogeneous correlationexactly. Instead, we will assume that $R_{ij}(y, \mathbf{r})$ is locally homogeneous at y. This of course implies that all our fitting parameters are functions of y.

It is known that the inertial range of $R_{ij}(y, \mathbf{r})$ in the log layer is self-similar, with a similarity variable r/y [12, 28]. To acknowledge this fact, the fitting volume $V_y' = \{\mathbf{r}; r_\epsilon(y) < r < r_L(y)\}$ is defined such that $r_L(y)$ is proportional to y near the wall (Fig. 9). Fig. 10 shows that the relative error in the model correlation is less than 20% throughout the channel. Also (Fig. 10), the isotropic component $\tilde{\mathbf{R}}^I(\mathbf{r})$ contributes the most, followed by $\tilde{\mathbf{R}}^b(\mathbf{r})$, $\tilde{\mathbf{R}}^d(\mathbf{r})$, $\tilde{\mathbf{R}}^Q(\mathbf{r})$, with the contribution from $\tilde{\mathbf{R}}^Q(\mathbf{r})$ being negligible. The Kolmogorov constant C_k calculated from a_1 has a value quite close to 2.0. In fact, this is true for the whole channel (Fig. 11), where $C_k(y)$ varies between 1.9 and 2.2. This can be explained from Fig. 12, where $\{p_b, p_d, p_Q\}$ can be seen to be larger than $p_I = 2/3$

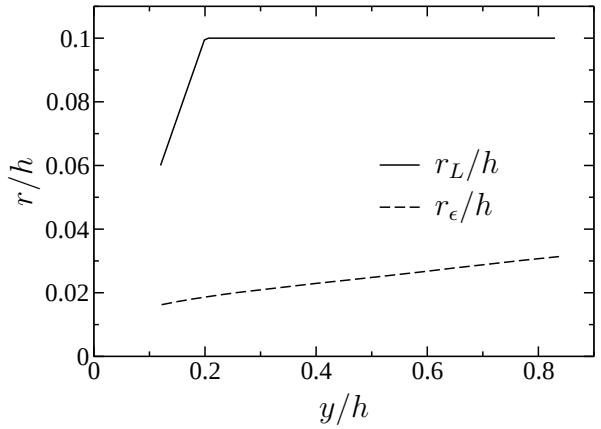

Figure 9: Upper and lower limits of the range of r over which error minimization is performed, for different y/h locations. The range is given by $r_\epsilon < r < r_L$, where $r_\epsilon(y) = (5C_k)^{3/4}\eta(y)$ and $r_L(y) = \min(y/2, 0.1)$

throughout the channel, satisfying the assumption of small-scale isotropy. Also consistent with this assumption is the fact that ϵ_{ij} is nearly isotropic.

The power-law exponents $p_b(y)$ and $p_d(y)$ are nearly constant throughout the channel and could be approximated as $p_b(y) \approx 1.4$ and $p_d(y) \approx 1$ (Fig. 12). The power-law exponent $p_Q(y)$ can be approximated as $p_Q(y) \approx 2.0$ up to $y/h = 0.5$ and then it starts to fluctuate near the center of the channel. This occurs because the contribution from $\tilde{\mathbf{R}}^Q$ is so small near the center of the channel that the total error $\|\mathbf{R}^{\text{MOD}} - \mathbf{R}^{\text{DNS}}\|$ is insensitive to large variations in p_Q. Qualitatively, (Fig. 13) the model fits the data quite well for the normal components, when the reference location ($y^+ = 114$) is in the log layer (Fig. 13). The inclination of principle axes are well represented and the magnitude of the contour levels match. The main shortcoming of the model lies in its inability to capture the effect of inhomogeneity, which is most obvious in the R_{12}^{DNS} component, where the isocontours of the DNS extend out further in the positive r_2 half of the plane as compared to the negative r_2 half, due to the presence of the wall. The model on the other hand is symmetric in $\mathbf{r}$, and is not able to capture this aspect of the data. This points to the need for modeling inhomogeneity in the representation.

3.2.4 Anisotropy due to Inhomogeneity

The results of fitting the homogeneous model to the inhomogeneous correlations from the channel flow (figure 13), clearly show the shortcomings on the homogeneous model in representing the cross-correlation R_{12}. Including inhomogeneity introduces significant complexity in the representation. One approach to this more complex formulation is described briefly below.

The inhomogenous two point correlation $R_{ij}(\mathbf{x}, \mathbf{x}') = \langle u_i(\mathbf{x}) u_j(\mathbf{x}') \rangle$ depends on two position vectors $\mathbf{x}$ and $\mathbf{x}'$, and can therefore also be mode to depend on any two linear combinations of these two position vectors. For instance, we could define $R_{ij}^{\eta}(\mathbf{y}, \mathbf{r}) = \langle u_i(\mathbf{x}) u_j(\mathbf{x}') \rangle$, where $\mathbf{y} = \eta\mathbf{x} + (1-\eta)\mathbf{x}'$ and $\mathbf{r} = \mathbf{x}' - \mathbf{x}$. R_{ij} satisfies the symmetry $R_{ij}(\mathbf{x}, \mathbf{x}') = R_{ji}(\mathbf{x}', \mathbf{x})$. It turns

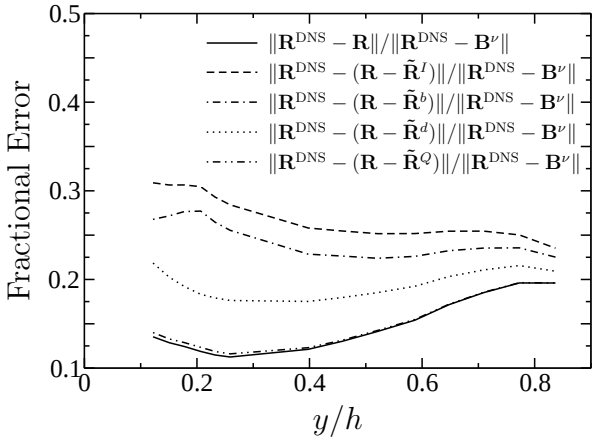

Figure 10: Fractional error of the model correlation with respect to the DNS correlation at various y/h locations across the channel. The bold curve shows the error of the total model correlation. The rest of the curves show the errors of the truncated model correlation at different y/h locations, with various components subtracted from the model correlation to form the truncated correlations.

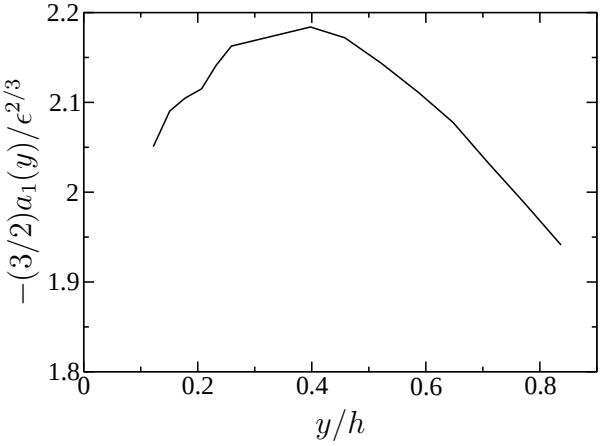

Figure 11: C_k obtained from $a_1(y)$

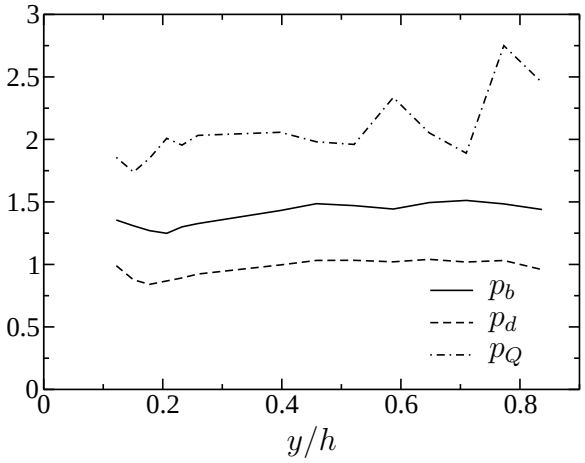

Figure 12: Power-law exponents $\{p_b, p_d, p_Q\}$ plotted for different y/h locations in the channel. p_I has been fixed at $2/3$ for the whole channel

out that the symmetry has the simplest form for $\eta = 1/2$, i.e. for $\mathbf{y} = (\mathbf{x} + \mathbf{x}')/2$, we have $R_{ij}^{1/2}(\mathbf{y}, \mathbf{r}) = R_{ji}^{1/2}(\mathbf{y}, -\mathbf{r})$. This form for the symmetry is easily satisfied by (for instance) a tensor that depends on $\mathbf{y}$, is even in $\mathbf{r}$ and is symmetric in ij.

The representation of $\langle u_i(\mathbf{x}) u_j(\mathbf{x}') \rangle$ is therefore best done in the mid-point coordinates ($\eta = 1/2$), because the symmetry conditions are easier to satisfy. From here, the $1/2$ superscript to denote the midpoint coordinate will be dropped.

Two-point correlation in the mid-point coordinate is $R_{ij}(\mathbf{y}, \mathbf{r}) = \langle u_i(\mathbf{y} - \mathbf{r}/2) u_j(\mathbf{y} + \mathbf{r}/2) \rangle$, and the two continuity conditions that need to be satisfied are:

$$\partial_j^+ R_{ij} = \left[\frac{1}{2} \frac{\partial}{\partial y_j} + \frac{\partial}{\partial r_j} \right] R_{ij} = 0 \tag{46}$$

$$\partial_i^- R_{ij} = \left[\frac{1}{2} \frac{\partial}{\partial y_i} - \frac{\partial}{\partial r_i} \right] R_{ij} = 0 \tag{47}$$

A form that satisties continuity can then be given as follows:

$$R_{ij}(\mathbf{y}, \mathbf{r}) = \epsilon_{ilk} \epsilon_{jmn} \partial_l^- \partial_m^+ \left[H_{kn}(\mathbf{r}, \mathbf{t}) a(\mathbf{y}) \right] \tag{48}$$

where t_{ij} is a tensor that satisfies $t_{kk} = 0$. The symmetry condition can be easily satisfied by assuming $H_{ij}(\mathbf{r}, \mathbf{t}) = H_{ji}(-\mathbf{r}, \mathbf{t})$. We also implicitly assume that t_{ij} does not vary with $\mathbf{y}$. That is, the relative strengths of the tensor components do not change with location. This is in fact a valid assumption for the anisotropies of the componentality and dimensionality tensors b_{ij} and d_{ij} in the log layer, where the correlation is self-similar. In this model, the inhomogenieties of B_{ij} and D_{ij} are then being manifested through the $\mathbf{y}$ dependence of $B_{ii}(\mathbf{y})$ and $D_{ii}(\mathbf{y})$ (which are not the same for inhomogenous turbulence).

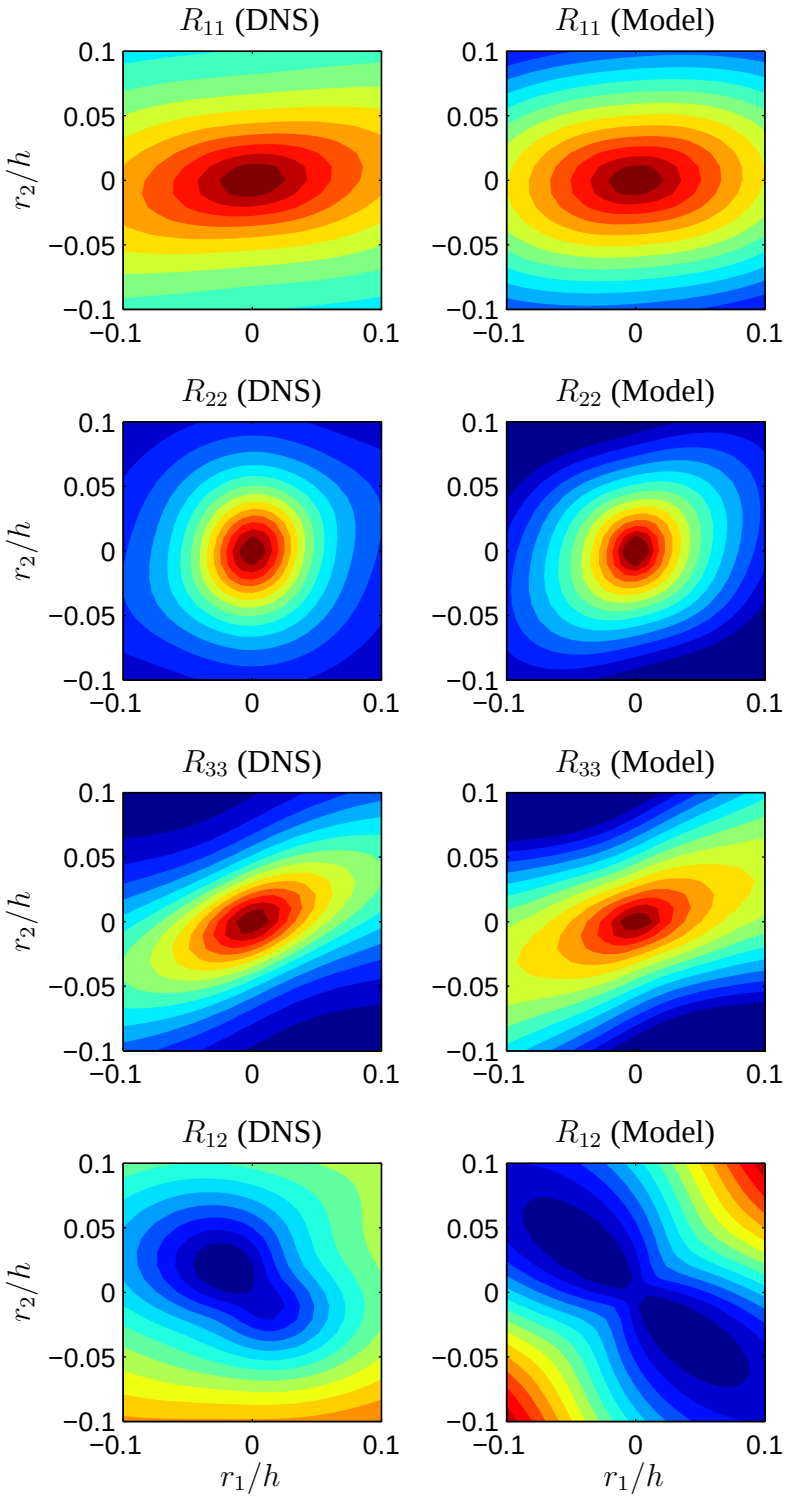

Figure 13: Isocontours of $R_{ij}^{\mathrm{DNS}}(y, \mathbf{r})$ (DNS) and $R_{ij}(y, \mathbf{r})$ (Model) at $y^+ = 114$, plotted for $r_z = 0$. The correlations in the left column were calculated from DNS of channel flow, and the correlation in the right column from the best fit of the model with DNS. The contour levels for a given correlation component (i.e. for the same row) have the same range.

Given $t_{ij} = t_{ji}$, four invariant forms for H_{ij} can be used:

$$\begin{aligned} H^1_{ij}(\mathbf{r},\mathbf{t}) &= f_1(r)t_{ij} && (49)\\ H^2_{ij}(\mathbf{r},\mathbf{t}) &= f_2(r)\delta_{ij}(\mathbf{r}\cdot\mathbf{t}\cdot\mathbf{r}) && (50)\\ H^3_{ij}(\mathbf{r},\mathbf{t}) &= f_3(r)r_ir_j(\mathbf{r}\cdot\mathbf{t}\cdot\mathbf{r}) && (51)\\ H^4_{ij}(\mathbf{r},\mathbf{t}) &= f_4(r)[r_i(\mathbf{r}\cdot\mathbf{t})_j + r_j(\mathbf{r}\cdot\mathbf{t})_i] && (52) \end{aligned}$$

Without any loss in generality, we also assume that the origin of $\mathbf{y}$ is at $(\mathbf{x}+\mathbf{x}')/2$, and model $a^\alpha(\mathbf{y})$ (which multiplies the corresponding H^α_{ij}) as a quadratic function in $\mathbf{y}$, i.e.

$$a^\alpha(\mathbf{y}) = c^\alpha + \lambda^\alpha_k y_k + A^\alpha_{st} y_s y_t \tag{53}$$

Note that since we are including all inhomogenous effects in $a^\alpha(\mathbf{y})$, if $c^\alpha = \beta c^\gamma$, then it implies that $\lambda^\alpha_k = \beta\lambda^\gamma_k$ and $A^\alpha_{st} = \beta A^\gamma_{st}$. That is, any constraints amongst $a^\alpha(\mathbf{y})$ will have to hold across its Taylor series expansion. Therefore, the inhomogenous representation of R_{ij} for a given t_{ij} is given by

$$R_{ij}(\mathbf{y},\mathbf{r}) = \sum_{\alpha=1}^{4} \epsilon_{ilk}\epsilon_{jmn}\partial^-_l\partial^+_m\left[H^\alpha_{kn}(\mathbf{r},\mathbf{t})a^\alpha(\mathbf{y})\right] \tag{54}$$

Expanding ∂^+ and ∂^-:

$$\begin{aligned} R_{ij}(\mathbf{y},\mathbf{r}) &= \sum_{\alpha=1}^{4}\epsilon_{ilk}\epsilon_{jmn}\left[\frac{1}{2}\frac{\partial}{\partial y_l} - \frac{\partial}{\partial r_l}\right]\left[\frac{1}{2}\frac{\partial}{\partial y_m} + \frac{\partial}{\partial r_m}\right]\left[H^\alpha_{kn}(\mathbf{r},\mathbf{t})a^\alpha(\mathbf{y})\right]\\ &= \sum_{\alpha=1}^{4}\epsilon_{ilk}\epsilon_{jmn}\left[\frac{1}{4}\frac{\partial}{\partial y_l}\frac{\partial}{\partial y_m} + \right.\\ &\quad \left.\frac{1}{2}\left\{\frac{\partial}{\partial r_m}\frac{\partial}{\partial y_l} - \frac{\partial}{\partial r_l}\frac{\partial}{\partial y_m}\right\} + \frac{\partial}{\partial r_l}\frac{\partial}{\partial r_m}\right]\left[H^\alpha_{kn}(\mathbf{r},\mathbf{t})a^\alpha(\mathbf{y})\right] \end{aligned} \tag{55}$$

$R_{ij}(0,\mathbf{r})$ can therefore be written as a sum of 3 terms:

$$R_{ij}(0,\mathbf{r}) = \underbrace{R^H_{ij}(\mathbf{r})}_{Homogeneous} + \underbrace{R^A_{ij}(\mathbf{r})}_{\text{Antisym Inhomog.}} + \underbrace{R^S_{ij}(\mathbf{r})}_{\text{Sym Inhomog.}} \tag{56}$$

where

$$
\begin{aligned}
R^H_{ij}(\mathbf{r}) &= \sum_{\alpha=1}^{4} \epsilon_{ilk}\epsilon_{jmn} \frac{\partial}{\partial r_l}\frac{\partial}{\partial r_m} H^\alpha_{kn}(\mathbf{r},\mathbf{t}) a^\alpha(0) \\
&= \sum_{\alpha=1}^{4} c^\alpha \epsilon_{ilk}\epsilon_{jmn} \frac{\partial}{\partial r_l}\frac{\partial}{\partial r_m} H^\alpha_{kn}(\mathbf{r},\mathbf{t}) = \sum_{\alpha=1}^{4} R^{H,\alpha}_{ij}(\mathbf{r}) \\
R^A_{ij}(\mathbf{r}) &= \sum_{\alpha=1}^{4} \epsilon_{ilk}\epsilon_{jmn} \frac{1}{2}\left[\left\{\frac{\partial}{\partial r_m}\frac{\partial}{\partial y_l} - \frac{\partial}{\partial r_l}\frac{\partial}{\partial y_m}\right\} H^\alpha_{kn}(\mathbf{r},\mathbf{t}) a^\alpha(\mathbf{y})\right]\Big|_{\mathbf{y}=0} \\
&= \sum_{\alpha=1}^{4} \epsilon_{ilk}\epsilon_{jmn} \frac{1}{2}\left\{\frac{\partial H^\alpha_{kn}(\mathbf{r},\mathbf{t})}{\partial r_m}\lambda^\alpha_l - \frac{\partial H^\alpha_{kn}(\mathbf{r},\mathbf{t})}{\partial r_l}\lambda^\alpha_m\right\} = \sum_{\alpha=1}^{4} R^{A,\alpha}_{ij}(\mathbf{r}) \\
R^S_{ij}(\mathbf{r}) &= \sum_{\alpha=1}^{4} \epsilon_{ilk}\epsilon_{jmn} \frac{1}{4}\left[\frac{\partial}{\partial y_l}\frac{\partial}{\partial y_m} H^\alpha_{kn}(\mathbf{r},\mathbf{t}) a^\alpha(\mathbf{y})\right]\Big|_{\mathbf{y}=0} \\
&= \sum_{\alpha=1}^{4} \epsilon_{ilk}\epsilon_{jmn} \frac{1}{4} A^\alpha_{lm} H^\alpha_{kn}(\mathbf{r},\mathbf{t}) = \sum_{\alpha=1}^{4} R^{S,\alpha}_{ij}(\mathbf{r})
\end{aligned}
$$

Here, $R^{H,\alpha}_{ij}$ are homogenous tensors, symmetric in $\mathbf{r}$ and ij, $R^{A,\alpha}_{ij}$ arises from the inhomogeniety (it has $\lambda^\alpha_{\mathbf{i}}$ in every term, arising out of first derivative of $a^\alpha(\mathbf{y})$), is antisymmetric in $\mathbf{r}$ and ij and $R^{S,\alpha}_{ij}$ also arises from the inhomogeniety (due to A^α_{ij}) and is symmetric in $\mathbf{r}$ and ij.

If all $R^{H,\alpha}_{ij}(\mathbf{r})$ have the same power law (i.e. $f_1 = r^p$, $f_2 = r^{p-2}$, $f_3 = r^{p-4}$ and $f_4 = r^{p-2}$), then it can be shown that $\{\mathbf{R}^{H,\alpha}\}$ are linearly dependent, and spanned by 2 tensors. However, it can also be shown that *all four tensors in* $\{\mathbf{R}^{S,\alpha}\}$ *will remain linearly independent.* Therefore, while satisfying the self-consistency condition, we can independently apply constraints for $R^{H,\alpha}_{ij}$ and $R^{S,\alpha}_{ij}$, even though they are both even functions in $\mathbf{r}$.

This representation was used to fit channel flow from the DNS at $Re_\tau = 940$ and the results for the normal components of the correlation tensor are the same. However, the antisymmetric part breaks the symmetry of the R_{12} component as shown in figure 14. This is an improvement over the results shown in figure 13, especially for small separations.

3.3 Generalization and Testing of Finite-Volume Wall-Bounded OLES

The application of OLES to general wall-bounded flows requires a synthesis of the wall-bounded OLES modeling pursued previously using spectral representations [39, 5] and the finite-volume formulation developed and evaluated for non-wall-bounded flows (see section 3.1 and [42, 26]). There were a number of unanticipated complications in this generalization of optimal LES, the two most important of which will be discussed here. These have been investigated in the context of statistical data obtained from direct numerical simulation of channel flow at $Re_\tau = 940$ [12].

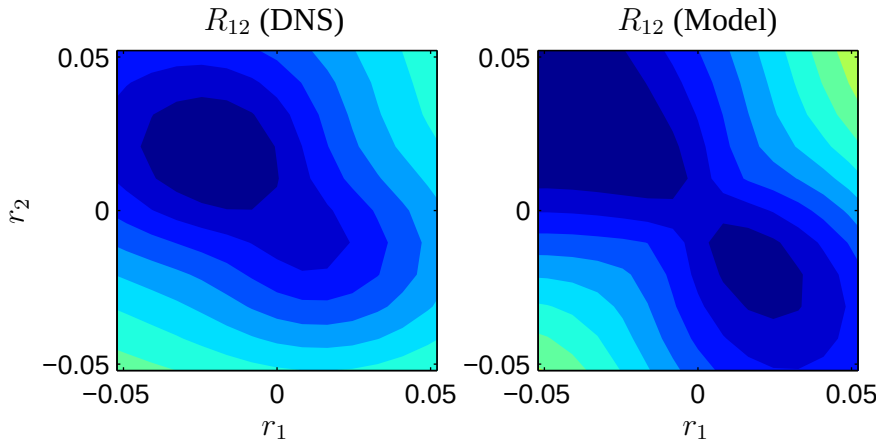

Figure 14: Isocontours of $R_{ij}^{\mathrm{DNS}}(y, \mathbf{r})$ (DNS) and $R_{ij}(y, \mathbf{r})$ (Model) at $y^+ = 114$, plotted for $r_z = 0$. The correlations on the left were calculated from DNS of channel flow, and the correlation in the right column from the best fit of the model with DNS. The contour levels have the same range.

3.3.1 The Spanwise Flux of Mean Momentum

As with the finite volume formulation described in section 3.1, in wall-bounded flows, the convective flux of momentum through the faces of the finite volumes is estimated using the sum of a quandratic and linear terms, where the linear term is expected to represent the transfer of energy to the unresolved scales. Using DNS statistical data, anisotropic OLES optimal models were developed on minimally sized stencils ($1 \times 1 \times 2$) for simplicty. In this inhomogeneous flow, the quadratic terms include the production of turbulent kinetic energy through interaction with the mean, in addition to the nonlinear turbulent cascade process. As a result, the quadratic term is a net producer of kinetic energy through much of the simulation domain. However, it was observed that the quadratic term slightly underestimated the rate of production in the central region of the channel. The model is guarenteed to correctly represent the energy transfers (*a priori*) so the linear term must make up for the missing production by being slightly anti-dissipative near the channel centerline. This is demonstrated in figure 15. The result when this model is used in an LES is an unstable simulation.

Further investigation of this phenomenon identified an unlikely culprit, the spanwise flux of mean streamwise momentum Uw' (U is the mean velocity and w' is the fluctuating spanwise velocity) that appears in the equation for streamwise velocity fluctuations u'. This is counter-intuitive because this term cancels out of the equation for $\langle u'^2 \rangle$. However, the OLES models ensure correct *a priori* values of many statistical quantities, including those involving this spanwise flux. In particular, the contribution of the quadratic term to the spanwise flux Uw' was underpredicted by the model and the linear term had to make up the difference. However, the form of the linear term, which involved only streamwise velocities was incompatible with the actual term Uw', which is linear in the (fluctuating) spanwise velocity. To correct this shortcoming, the model was generalized to include a linear in w' term in them streamise momentum equations, and this resulted in a stable simulation. The near-wall velocity variances from this simulation are shown in figure 16.

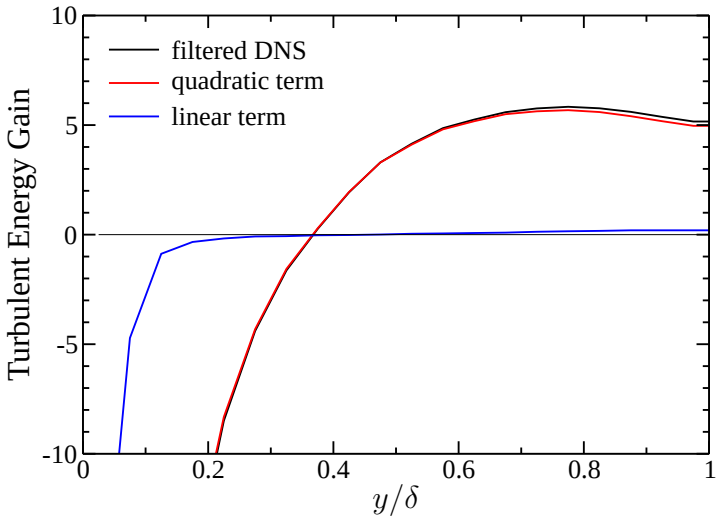

Figure 15: Streamwise energy production and destruction through the uw term by the LES convective terms in the channel as determined from the filtered DNS, the quadratic model term and the linear model term.

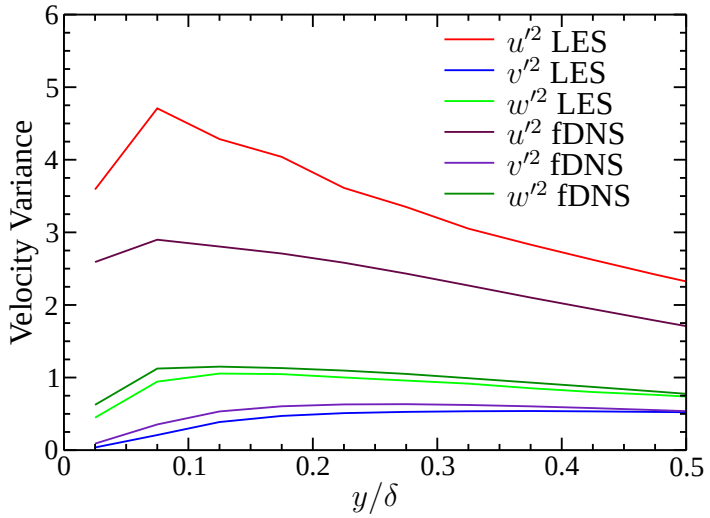

Figure 16: Velocity variances from the filtered DNS (fDNS) and the optimal LES (LES).

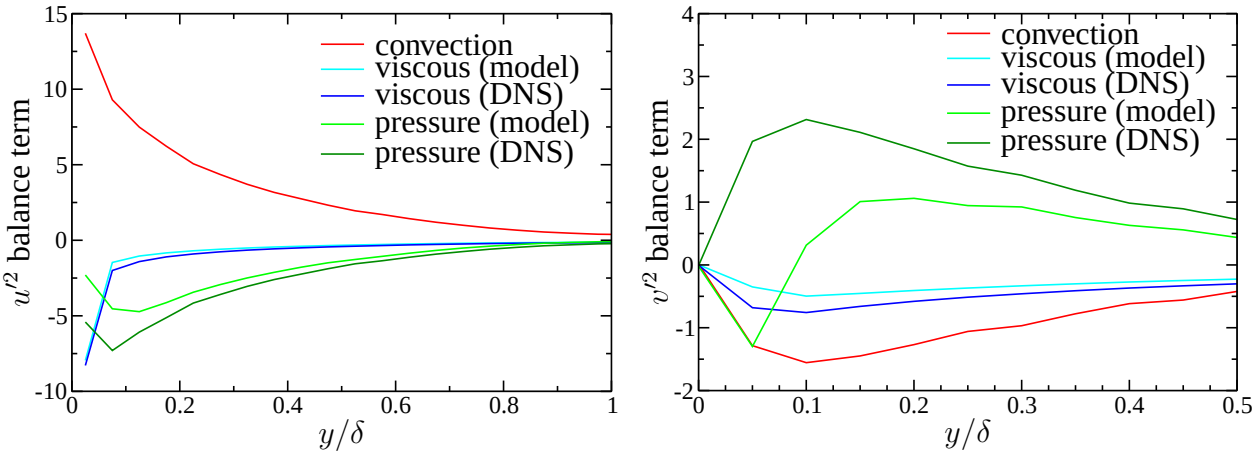

Figure 17: Contribution of the convection, viscous and pressure terms to the evolution of the filtered velocity variances as determined from the filtered DNS and optimal LES model.

3.3.2 Near-wall Pressure Contributions

The obvious shortcoming of the LES results shown in figure 16 is that the streamwise fluctuations are over-predicted compared to the filtered DNS, and the other velocity fluctuation components are somewhat underpredicted. A likely source of this discrepency is shown in figure 17 in which the agregated terms in the evolution equations for $\langle u'^2 \rangle$ and $\langle v'^2 \rangle$ are shown. Notice that the primary discrepency between the LES model terms and the DNS terms is in the pressure contribution, which is responsible for the transfer of energy from the streamwise to the other velocity components.

In this OLES model formulation, the pressure is determined by imposing a discrete divergence free-constraint on the volume averaged velocities, as in a standard staggered grid finite volume scheme. This is a modeling ansatz is based on the observations of [20] that in finite volume LES of isotropic turbulence this is very nearly the the optimal model. The presence of the wall appears to be upsetting that conclusion. There are several ways to interpret the discrepency in the pressure term. The most useful is to observe that the magnitude of the discrete divergence of the convective term is greatly underestimated by the model relative to the filtered DNS (figure 18), resulting in a lower pressure contribution. This is a property of the convective terms that the OLES formulation does not control for. The proposed solution to this problem is to reformulate the OLES model to estimate the (discrete) divergence-free projection of the convection term. This proposal is currently being evaluated.

3.4 Conclusions

3.4.1 Theory-based Finite-Volume OLES

The correlations required for the finite-volume OLES formulation can be obtained from Kolmogorov inertial-range theory, small-scale isotropy, and the quasi-normal approximation. Further, LES models resulting from these correlations perform well. These approximations will be valid

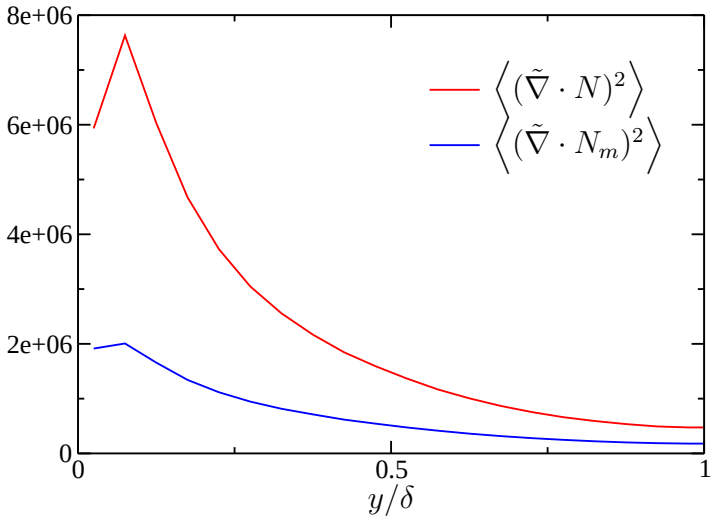

Figure 18: Variance of the divergence of the LES convection term N, as determined from the DNS (N)and the optimal LES model (N_m).

provided the turbulence at the filter scale and smaller is locally homogeneous and isotropic. Except for very near walls and other strong inhomogeneities, this is expected to be a good approximation provided the Reynolds number is sufficiently high and the filter width is sufficiently small.

The finite-volume OLES models developed here are expressed as discrete quadratic and linear operators that represent the convective momentum flux. These operators depend explicitly on two flow dependent parameters: the dissipation rate ϵ and the nondimensional parameter $\gamma = \Delta\epsilon/u^3$ (the ratio of the grid size Δ to the large turbulence scale). The modeling approach allows the parameters ϵ and u^2 to be determined dynamically and accurately in a running LES. But it was also found that asymptotic operators for $\gamma \to 0$ yield results consistent with the finite γ operators with γ as large as 0.08. In most cases, therefore, the asymptotic operators are sufficiently accurate, meaning that only ϵ needs be determined dynamically. The process for determining ϵ is considerably simpler than the usual dynamic procedure [13], as no test filter is required.

The quadratic and linear operators arising from the LES optimization are broadly similar to common finite-volume operators. However, there are significant quantitative differences between the OLES operators and standard finite-volume operators, which should be interpreted as part of the model for the effects of subgrid scales. The linear part of the operators, which play the role of the subgrid stress model by dissipating resolved energy, are different for the normal and tangential velocity components in any grid direction, with the tangential component dissipation significantly lower at high wavenumbers than a standard fourth-order approximation to the second derivative. This is one of the features of the OLES approach; the spectral distribution of subgrid dissipation is tailored to be consistent with the statistics of turbulence. Finally, note that the quadratic OLES operators on average produce resolved-scale energy and the linear operators dissipate energy. The dissipation of the linear term is determined to ensure that the combined contributions of quadratic and linear terms to the resolved energy evolution match the required total dissipation.

These results indicate that practical finite-volume OLES models can be formulated without DNS correlation inputs, at least for the circumstances for which most LES models are designed (small-

scale isotropy). The advantage of the current formulation is that it allows the effects of subgrid turbulence and numerical discretization to be treated in a unified way and consistent with the statistical properties of turbulence. It is both remarkable and encouraging that the simple considerations employed here are sufficient for this modeling.

Several immediate generalizations are possible using the isotropic statistical models introduced here. These include LES of scalar transport and modeling on anisotropic and inhomogeneous grids, as one would encounter in most applications. Also important is the generalization to anisotropic correlations for LES models applicable when isotropy at the grid scale is not a valid assumption. This occurs, for example, in near-wall turbulence. Isotropy places a strong constraint on the form of the multi-point correlations. Without isotropy, even the two-point second-order correlation is difficult to represent (see [6] and the references therein). The possibility raised in section 3.1.6 that the I^3 contribution to the OLES estimation equations might be neglected or crudely modeled is thus particularly important, since the underlying three-point third-order correlation is the most difficult to model. However, the robustness of this result to anisotropy and inhomogeneity of the turbulence and the LES grid is far from clear.

3.4.2 Modeling Anisotropy of Two-point Correlations

The results show that the homogeneous model fits the correlations calculated from DNS data rather well, both quantitatively and qualitatively, though there are shortcomings to the fit, arising from limitations of the model. In particular, to improve the representation of the small separation correlations discussed here for flows that are inhomogeneous, the effects of the inhomogeneity on the correlation needs to be represented, particularly the breaking of the symmetry expressed as $R_{ij}(\mathbf{r}) = R_{ij}(-\mathbf{r})$. A preliminary inhomogeneous formulation was proposed and tested, with encouraging results.

The primary advantage of models of the type developed here for the small separation correlation is that they have a finite number of parameters (17 including the power-law exponents for the homogeneous model). If we neglect the part of the correlation depending on Q^*_{ijk} (which accounts for $< 5\%$ of the correlation), then our model can be expressed in terms of just 9 free parameters. A similar SO(3) (up to $l = 2$) decomposition for $R_{ij}(\mathbf{r})$ that has even parity in $\mathbf{r}$, is symmetric in ij and satisfies the homogenous continuity equation will have 8 free parameters [2] (after fixing the isotropic power law) – thus, the number of DOFs in our model is comparable to that of the simplest possible anisotropic SO(3) representation. At any rate, a finite number of measurements of the correlation will be sufficient to parametrize our model, effectively reconstructing the correlation from a small amount of data. This is useful in interpreting experimental data, but perhaps more important, it is useful for reconstructing the turbulence correlations from correlations computed from a large eddy simulation. Applying the LES filter to the correlation model yields a representation of the correlation of the LES velocities, which can be fit to the LES data similar to the fits to DNS performed in this paper. The parameters so determined, when applied to the unfiltered correlation representation, define the turbulence correlation consistent with the correlations of the LES fields.

Seventeen is a large number of parameters, which raises the questions as to how practical it might be to parametrize such a model using LES (or experimental) data. However, this is a second rank correlation tensor. Correlations for just two non-zero values of $\mathbf{r}$ yield 18 data items. If the

correlation (or the filtered correlation) is sampled on a rectangular grid (e.g. an LES grid), with nearest neighbor separations (7 points total) that would amount to 33 data items (accounting for symmetries), and sampling on a cubical grid of 27 separations yields 123 independent data items. Clearly, data from a reasonable number of small separations should be sufficient to parametrize the model. An effort to extract R_{ij} in this manner from LES statistics was undertaken by Bhattacharya [4], where encouraging results were obtained for extracting the normal Reynolds stress components $B_{\alpha\alpha}$ from LES correlations.

While the results described above are encouraging for the representation of anisotropy in the two-point second-order velocity correlation, the optimal LES formulation also needs a model for the three-point third-order correlation. The complexity of such a model will be much greater than for the two-point correlation discussed here, so much so that this approach to anisotropy representation of the correlations underlying the LES formulation now appear impractical. The current results for the two-point correlation will be useful for reconstructing second order statistics from LES fields, but another approach to representing the anisotropy in optimal LES models appears to be needed.

A much more direct and simplier approach is currently being pursued. It is based on the modeling ansatz that the anisotropy of the interaction between rsolved and unresolved scales can be characterized by anisotropy in the dissipation inferred from an LES using the techniques described in [26]. This approach is currently being evaluated for its effectiveness.

3.4.3 Finite Volume Wall-bounded OLES

The execution of finite volume OLES for wall-bounded turbulence encountered several unanticipated roadblocks, which have been or are being overcome. As with previous development of OLES models, the resolution of the problems encountered was facilitated by the formal structure of the modeling approach, which provides a theoretical framework in which the expectations for the statistical properties of the model are analyzed. The analysis also provides insight with potential application for wall-bounded LES in general. In particular, one of the common shortcomings of wall-bounded LES, especially with unresolved wall layers, is the over prediction of streamwise velocity fluctuations, just as observed here. It may be that this shortcoming is commonly related to inadequacies in the treatment of pressure and the continuity constraint, as is the case here.

4 Other Information

This project was sponsored by AFOSR under the subject grant. The following personnel were supported under this grant:

Amitabh Bhattacharya	Postdoc, University of Texas at Austin
	Current Position: Postdoc University of Pittsburgh
Henry Chang	Graduate student, University of Texas at Austin
Nicholas Malaya	Graduate student, University of Texas at Austin
	Current Position: Research Engineer, University of Texas at Austin
Robert D. Moser	Professor, University of Texas at Austin
Julie Siloti	Graduate student, University of Texas at Austin

A number of papers were published during the grant period based on research undertaken under this grant, and its predecessor. These are listed below:

Publications

Moser, R. D., Malaya, N. P., Chang, H., Zandonade, P. S., Vedula, P., Bhattacharya, A. & Haselbacher, A. 2009 Theoretically based optimal large-eddy simulation, *Phys. of Fluids*, **21**, 105104.

Bhattacharya, A., Das, A. & Moser, R. D. 2008 A filtered-wall formulation for large-eddy simulation of wall-bounded turbulence, *Phys. of Fluids*, **20**, 115104.

Bhattacharya, A., Kasinos, S. & Moser, R. D. 2008 Representing anisotropy of two-point second-order turbulence velocity correlations using structure tensors, *Phys. of Fluids*, **20**, 101502.

Chang, H. & Moser, R. D. 2007 An inertial range model for the three-point third-order velocity correlation *Physics of Fluids*, **19**, 105111.

Acknowledgment/Disclaimer

This work is sponsored by the Air Force Office of Scientific Research, USAF, under grant/contract number F9550-07-1-0411. The views and conclusions contained herein are those of the authors and should not be interpreted as necessarily representing the official policies or endorsements, either expressed or implied, of the Air Force Office of Scientific Research or the U. S. Government.

References

[1] R. Adrian, B. Jones, M. Chung, Y. Hassan, C. Nithianandan, and A. Tung. Approximation of turbulent conditional averages by stochastic estimation. *Physics of Fluids*, 1(6):992–998, 1989.

[2] Itai Arad, Victor S. L'vov, and Itamar Procaccia. Correlation functions in isotropic and anisotropic turbulence: The role of the symmetry group. *Phys. Rev. E*, 59(6):6753–6765, Jun 1999.

[3] G. K. Batchelor. *The theory of homogeneous turbulence*. Cambridge Univ. Press, Cambridge, England, 1953. pg. 53.

[4] A. Bhattacharya. *Towards Optimal Large-Eddy Simulation of Wall-Bounded Flows*. PhD thesis, University of Illinois, Urbana-Champaign, 2007.

[5] A. Bhattacharya, A. Das, and R. D. Moser. A filtered-wall formulation for large-eddy simulation of wall-bounded turbulence. *Phys. of Fluids*, 20:115104, 2009.

[6] A. Bhattacharya, S. Kassinos, and R. D. Moser. Representing anisotropy of two-point second-order turbulence velocity correlations using structure tensors. *Phys. of Fluids*, 20, 2008.

[7] L. Biferale, E. Calzavarini, F. Toschi, and R. Tripiccione. Universality of anisotropic fluctuations from numerical simulations of turbulent flows. *Europhysics Letters*, 64(4):461–467, 2003.

[8] L. Biferale, D. Lohse, I.M. Mazzitelli, and F. Toschi. Probing structures in channel flow through SO(3) and SO(2) decomposition. *Journal of Fluid Mechanics*, 452:39–59, 2002.

[9] Henry Chang and Robert D. Moser. An inertial range model for the three-point third-order velocity correlation. *Physics of Fluids*, 19:105111, 2007.

[10] D. R. Chapman. Computational aerodynamics, development and outlook. *AIAA Journal*, 17:1293–1313, 1979.

[11] Arup Das. *A Filtered Wall Formulation for Large-Eddy Simulation of Wall-Bounded Turbulence*. PhD thesis, University of Illinois at Urbana-Champaign, Urbana, IL, 2004.

[12] J.C. Del Álamo, J. Jiménez, P. Zandonade, and R.D. Moser. Scaling of the energy spectra of turbulent channels. *Journal of Fluid Mechanics*, 500:135–144, 2004.

[13] M. Germano, U. Piomelli, P. Moin, and W. Cabot. A dynamic subgrid-scale eddy viscosity model. *Physics of Fluids*, 3:1760–1765, 1991.

[14] S.C. Kassinos, W.C. Reynolds, and M.M. Rogers. One-point turbulence structure tensors. *Journal of Fluid Mechanics*, 428:213–248, 2001.

[15] A. N. Kolmogorov. Dissipation of energy in locally isotropic turbulence. *Dokl. Akad. Nauk SSSR*, 32:16–18, 1941. reprinted in *Proc. R. Soc. Lond. A* **434** 15-17 (1991).

[16] A. N. Kolmogorov. The local structure of turbulence in incompressible viscous fluid for very large Reynolds numbers. *C. R. Acad. Sci. URSS*, 30:301, 1941.

[17] R. H. Kraichnan. Relation of fourth-order to second-order moments in stationary isotropic turbulence. 107:1485–1490, 1957.

[18] S. Kurien and K.R. Sreenivasan. Anisotropic scaling contributions to high-order structure functions in high-Reynolds-number turbulence. *Physical Review E*, 62(2):2206–2212, 2000.

[19] J. Langford and R. Moser. Optimal LES formulations for isotropic turbulence. *Journal of Fluid Mechanics*, 398:321–346, 1999.

[20] J. A. Langford and R. D. Moser. Breakdown of continuity in large-eddy simulation. *Physics of Fluids*, 11:943–945, 2001.

[21] M. Lesieur. *Turbulence in Fluids*. Kluwer Academic Publishers, Dordrecht, 3rd edition, 1997.

[22] I. Mary and P. Sagaut. Large eddy simulation of flow arouond an airfoil near stall. *AIAA J.*, 40:1139–1145, 2002.

[23] C. P. Mellen, J. Frohlich, and W. Rodi. Lessons from lesfoil project on large-eddy simulation of flow around an airfoil. *AIAA Journal*, 41(4):573–581, 2003.

[24] A. S. Monin and A. M. Yaglom. *Statistical Fluid Mechanics: Mechanics of Turbulence, Volume II*. Dover, 1975. pg. 70.

[25] R. D. Moser, A. Das, and A. Bhattacharya. Filtering the wall as a solution to the wall-modeling problem. In *Proceedings of Complex Effects in Large Eddy Simulation, Sept. 20-24, 2005, Limasol, Cyprus*, 2006.

[26] R. D. Moser, N. P. Malaya, H. Chang, P. S. Zandonade, P. Vedula, A. Bhattacharya, and A. Haselbacher. Theoretically based optimal large-eddy simulation. *Phys. of Fluids*, 21:105104, 2009.

[27] F. Nicoud, J. S. Baggett, P. Moin, and W. Cabot. Large eddy simulation wall-modeling based on suboptimal control theory and linear stochastic estimation. *Physics of Fluids*, 13:2968–2984, 2001.

[28] M. Oberlack. Symmetries in turbulent boundary layer flows. In *Center for Turbulence Research Annual Research Briefs – 1996*, pages 183–197, Stanford, CA, 1996. Stanford University.

[29] Y. Ogura. A consequence of the zero-fourth-cumulant approximation in the decay of isotropic turbulence. *Journal of Fluid Mechanics*, 16:33–40, 1963.

[30] S. Orszag. Analytical theories of turbulence. *Journal of Fluid Mechanics*, 41(2):363–386, 1970.

[31] U. Piomelli and E. Balaras. Wall-layer models for large-eddy simulations. *Ann. Rev. Fluid Mech.*, 34:349–374, 2002.

[32] U. Piomelli, J. Ferziger, P. Moin, and J. Kim. New approximate boundary-conditions for large eddy simulations of wall-bounded flows. *Physics of Fluids*, 6:1061–1068, 1989.

[33] I. Proudman and W. H. Reid. On the decay of a normally distributed and homogeneous turbulent velocity field. *Phil. Trans. R. Soc. Lond. A*, 247:163–189, 1954.

[34] W. C. Reynolds. The potential and limitations of direct- and large-eddy simulations. In J. L. Lumley, editor, *WIther Turbulence? Turbulence at the Crossroads*, pages 313–342. Springer, Heidelberg, 1990.

[35] A.J.M. Spencer. Theory of invariants. In A.C.Eringen, editor, *Continuum Physics*, volume 1. New York, Academic Press, 1971.

[36] K.R. Sreenivasan. On the universality of the Kolmogorov constant. *Physics of Fluids*, 7:2778, 1995.

[37] J. A. Templeton, M. Wang, and P. Moin. An efficient wall model for large-eddy simulation based on optimal control theory. *Physics of Fluids*, 18, 2006.

[38] P. Vedula, R. D. Moser, and P. S. Zandonade. On the validity of quasi-normal approximation in turbulent channel flow. *under review for Phys. Fluids*, 2005.

[39] S. Volker, P. Venugopal, and R. D. Moser. Optimal large eddy simulation of turbulent channel flow based on direct numerical simulation statistical data. *Physics of Fluids*, 14:3675, 2002.

[40] T. von Kármán and L. Howarth. On the statistical theory of isotropic turbulence. *Proc. R. Soc. London A*, 164:192, 1938.

[41] M. Wang and P. Moin. Dynamic wall modeling for large-eddy simulation of complex turbulent flows. *Physics of Fluids*, 14:2043–2051, 2002.

[42] P.S. Zandonade, J.A. Langford, and R.D. Moser. Finite volume optimal large-eddy simulation of isotropic turbulence. *Physics of Fluids*, 16:2255–2271, 2004.